Dalton Transactions

PAPER

Cite this: DOI: 10.1039/c6dt03425j

Vanadium(IV and V) complexes of pyrazolone based ligands: Synthesis, structural characterization and catalytic applications†

Mannar R. Maurya,*[a] Bithika Sarkar,[a] Fernando Avecilla[b] and Isabel Correia*[c]

The ONO donor ligands obtained from the condensation of 4-benzoyl-3-methyl-1-phenyl-2-pyrazoline-5-one (Hbp) with benzoylhydrazide (H_2bp-bhz **I**), furoylhydrazide (H_2bp-fah **II**), nicotinoylhydrazide (H_2bp-nah **III**) and isonicotinoylhydrazide (H_2bp-inh **IV**), upon treatment with $[V^{IV}O(acac)_2]$, lead to the formation of $[V^{IV}O(bp\text{-}bhz)(H_2O)]$ **1**, $[V^{IV}O(bp\text{-}fah)(H_2O)]$ **2**, $[V^{IV}O(bp\text{-}nah)(H_2O)]$ **3** and $[V^{IV}O(bp\text{-}inh)(H_2O)]$ **4**, respectively. At neutral pH the *in situ* generated aqueous $K[H_2V^{V}O_4]$ reacts with ligands **I** and **II**, forming potassium salts, $K(H_2O)_2[V^{V}O_2(bp\text{-}bhz)]$ **5** and $K(H_2O)_2[V^{V}O_2(bp\text{-}fah)]$ **6**, while ligands **III** and **IV** give neutral complexes, $[V^{V}O_2(bp\text{-}nah)]$ **9** and $[V^{V}O_2(bp\text{-}inh)]$ **10**, respectively. Acidification of aqueous solutions of **5** and **6** with HCl also gives neutral complexes $[V^{V}O_2(Hbp\text{-}bhz)]$ **7** and $[V^{V}O_2(Hbp\text{-}fah)]$ **8**, respectively. Complexes **1–4**, upon slow aerial oxidation in methanol, convert into monooxidovanadium(V) complexes, $[V^{V}O(bp\text{-}bhz)(OMe)]$ **11**, $[V^{V}O(bp\text{-}fah)(OMe)]$ **12**, $[V^{V}O(bp\text{-}nah)(OMe)]$ **13** and $[V^{V}O(bp\text{-}inh)(OMe)]$ **14**, respectively. All complexes were characterized by various spectroscopic techniques like FT-IR, UV-visible, EPR (for complexes **1–4**) and NMR (^{1}H, ^{13}C and ^{51}V), elemental analysis, thermogravimetry and single crystal X-ray diffraction (for complexes **5**–**10** and **12**). In the solid state, all complexes characterized by X-ray diffraction show the metal ion 5-coordinated in a distorted square pyramidal geometry. Complexes **11–14** were tested as catalysts for the one-pot three-component (ethylacetoacetate, benzaldehyde and ammonium acetate) dynamic covalent assembly, *via* Hantzsch reaction, using hydrogen peroxide as oxidant in solution and under solvent-free conditions. The complexes are also active catalysts for the oxidation of tetralin to tetralone with H_2O_2 as oxidant. The influence of the amounts of catalyst and oxidant, and solvent, temperature and time on the catalyzed reactions was investigated.

Received 1st September 2016,
Accepted 15th September 2016

DOI: 10.1039/c6dt03425j

www.rsc.org/dalton

Introduction

Hantzsch 1,4-dihydropyridines (1,4-DHPs) are one of the most significant groups of heterocyclic compounds because of their pharmacological activity as calcium antagonists or agonists.[1] Substituted 1,4-DHPs are extensively used in other pharmacological applications such as antitumor,[2] bronchodilating[3] antidiabetic,[4] neurotropic[5] and antianginal.[6] First reported in 1882, the Hantzsch reaction is a convenient way to prepare 1,4-DHPs, involving the condensation of an aldehyde with 2 equivalents of a β-keto ester and a nitrogen donor.[7] Aromatization of DHPs has received considerable attention because the conversion of 1,4-DHPs into the corresponding pyridine derivatives is one of the main metabolic pathways of the above drugs. 1,4-DHP based calcium-channel blockers are oxidatively converted into pyridine derivatives by cytochrome P-450 in the liver[8] and these show anti-hypoxic and anti-ischemic activities.[9] In recent years, Bocker and co-workers[10] have studied the metabolism of Hantzsch 1,4-DHPs and showed that the first metabolic step includes aromatization to the corresponding pyridine derivative. Moreover, the products of aromatization (substituted pyridines) have found use in the treatment of atherosclerosis and various coronary diseases.[11] Therefore, the oxidative aromatization of DHPs has attracted substantial attention from organic and medicinal chemists. Numerous reagents and procedures have been suggested for the oxidation of DHPs. Strong oxidizing reagents such as pyridinium chlorochromate,[12] metallic salts *e.g.* $Zr(NO_3)_4$,[13] $(NH_4)_4Ce(NO_3)_6$,[14] urea nitrate, photochemical oxidation[15] silver salts, iodine monochloride, inorganic acidic salts,[16]

[a]*Department of Chemistry, Indian Institute of Technology Roorkee, Roorkee-247667, India. E-mail: rkmanfcy@iitr.ernet.in; Fax: +91 1332 273560; Tel: +91 1332 285327*
[b]*Departamento de Química Fundamental, Universidade da Coruña, Campus de A Zapateira, 15071 A Coruña, Spain*
[c]*Centro de Química Estrutural, Instituto Superior Técnico, Universidade de Lisboa, Av. Rovisco Pais 1, 1049-001 Lisboa, Portugal. E-mail: icorreia@ist.utl.pt; Fax: +35 121 8464455; Tel: +351 21 8419177*

† Electronic supplementary information (ESI) available: Details of EPR, ^{51}V NMR and other spectroscopic studies. CCDC 1502023–1502029. For ESI and crystallographic data in CIF or other electronic format see DOI: 10.1039/c6dt03425j

sodium nitrite/nitrate and O_2-activated carbon have been used.[17] However, most of the reported oxidation procedures involve long reaction times, strong oxidizing agents in large excess, low selectivity and yield, harsh reaction condition, use of toxic and expensive reagents, corrosive solvents, tedious work-ups, *etc*. Furthermore, the aromatization leads to dealkylation of the 4-position or formation of side products.[18] Therefore, the development of more efficient and mild methods for the aromatization of DHPs is still required. Recently, it has been reported that manganese Schiff base complexes,[19] cobalt silica grafted complexes,[20] $MoOCl_4$,[21] $SbCl_5$ [22] and vanadium salts[23] can be used as catalysts in the presence of the mild oxidant H_2O_2 for aromatization and all these processes produce higher yields in lower reaction times.

Among various transition metals, vanadium has been extensively used in catalytic oxidation reactions of various organic substrates including sulphoxidation,[24] bromination,[25] oxidation of alcohols,[26] epoxidation of olefins,[27] hydroxylation of aromatic hydrocarbons,[28] *etc*. However, to the best of our knowledge, aromatization by vanadium azine complexes has not been reported. Therefore, we have synthesized oxidovanadium(IV), oxidovanadium(V) and dioxidovanadium(V) complexes of pyrazolone based ligands (Scheme 1) and used the oxidovanadium(V) complexes for a milder and more selective catalyzed aromatization of 1,4-DHPs.

We have also extended the catalyst scope towards the selective oxidation of tetralin to tetralone. Tetralone is a ketohydronaphthalene which is used as a reactive intermediate in dyes, pharmaceuticals, and agrochemicals.[29,30] Tetralone can be prepared by Friedel–Crafts acylation of aromatics with acid halide/anhydride or oxidation reactions. The corrosive $AlCl_3$ as catalyst or $KMnO_4/K_2Cr_2O_7$ as oxidizing agent have been used in both processes.[31] Many studies have been put forward recently on the development of environmentally friendly and economically sustainable processes for the selective oxidation of alkylaromatics and cycloalkanes to higher value-added ketones. In this scope, catalytic systems (homogeneous and heterogeneous) involving "green" oxidants like O_2 and H_2O_2 have been developed for the oxidation of tetralin.[32,33] In the present work, we have used oxidovanadium(V) complexes as catalysts for the oxidation of tetralin by H_2O_2 at 80 °C.

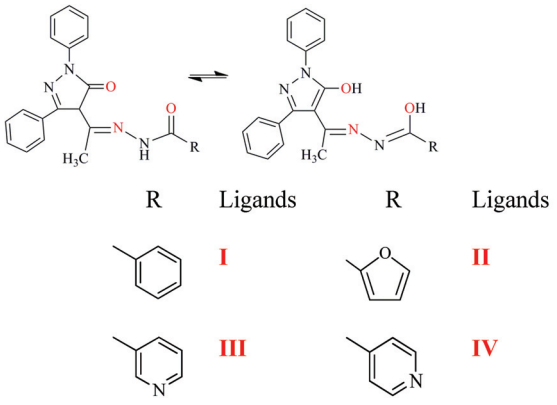

Scheme 1 Structure of pyrazolone based ligands used in this study.

Experimental section

Materials and methods

Acetylacetone, furoylhydrazide (Aldrich Chemicals Co., USA), ethylbenzoate, hydrazine hydrate, isonicotinoylhydrazide (Loba Chemie, Mumbai, India), nicotinoylhydrazide (Acros Organics, New Jersey, USA), ethylacetoacetate, ammonium acetate, diethylether, benzaldehyde, tetraline and 30% aqueous H_2O_2 (Renkem, India) were used as received. Other chemicals and solvents were of analytical reagent grade. $[V^{IV}O(acac)_2]$[34] and the ligands H_2bp-bhz **I**, H_2bp-fah **II**, H_2bp-nah **III** and H_2bp-inh **IV**[35] were prepared according to methods reported in the literature.

Instrumentation

Elemental analyses (C, H and N) were carried out using an Elementar model Vario-E1 III. IR spectra were recorded as KBr pellets on a Nicolet 1100 FT-IR spectrometer after grinding the samples. Electronic absorption spectra were recorded in methanol with a Shimadzu UV-1601 PC UV-visible spectrophotometer. ^{1}H and ^{13}C NMR spectra were recorded in DMSO-d_6 on a Bruker Advance 500 MHz spectrometer. ^{51}V NMR spectra were recorded on a Bruker Avance III 400 MHz instrument. ^{51}V chemical shifts were referenced relative to neat $V^{V}OCl_3$ as the external standard. EPR spectra were recorded with a Bruker ESP 300E X-band spectrometer coupled to a Bruker ER041 X-band frequency meter (9.45 GHz). The complexes were dissolved at room temperature in DMSO p.a. grade, previously degassed by passing N_2 for 10 min, to obtain *ca*. 3 mM solutions. Spectra were recorded at 77 K and simulated with a program developed by Rockenbauer and Korecz.[36] Thermogravimetric analyses of the complexes were carried out under an oxygen atmosphere using a TG Stanton Redcroft STA 780 instrument. A Shimadzu 2010 plus gas-chromatograph fitted with an Rtx-1 capillary column (30 m × 0.25 mm × 0.25 μm) and a FID detector was used to analyze the reaction products and their quantification was done based of the relative peak area of each product. The identity of the products was confirmed using a GC-MS model Perkin-Elmer Clarus 500 and by comparing the fragments of each product with the library available.

Preparation of the complexes

$[V^{IV}O(bp\text{-}bhz)(H_2O)]$ 1. The ligand H_2bp-bhz (0.34 g, 0.0010 mol) was dissolved in absolute methanol (15 mL) and filtered. A solution of $[V^{IV}O(acac)_2]$ (0.26 g, 0.0010 mol) in methanol (15 mL) was added to the above solution with stirring. The reaction mixture was refluxed for 4 h. The final solution was reduced to 10 ml and kept in the fridge. Gradually a black solid precipitated, which was filtered, washed with

methanol followed by petroleum ether (b.p. 60 °C) and dried in a desiccator over silica gel. Yield: 0.36 g (75%). Found: C, 60.2; H, 4.4; N, 11.6; $C_{24}H_{20}N_4O_4V$ (479.38 g mol^{-1}) requires C, 60.13; H, 4.21; N, 11.69.

$[V^{IV}O(bp\text{-}fah)(H_2O)]$ 2, $[V^{IV}O(bp\text{-}nah)(H_2O)]$ 3 and $[V^{IV}O(bp\text{-}inh)(H_2O)]$ 4. Complexes **2–4** were prepared from H_2bp-fah **II**, H_2bp-nah **III** and H_2bp-inh **IV**, respectively, following the method outlined for **1**.

2: Yield: 0.39 g (83%). Found: C, 56.5; H, 4.0; N, 11.8; $C_{22}H_{18}N_4O_5V$ (469.34 g mol^{-1}) requires C, 56.30; H, 3.87; N, 11.9.

3: Yield: 0.34 g (71%). Found: C, 57.5; H, 3.8; N, 14.6; $C_{23}H_{19}N_5O_4V$ (480.37 g mol^{-1}) requires C, 57.51; H, 3.99; N, 14.58.

4: Yield: 0.36 g (75%). Found: C, 57.1; H, 3.7; N, 14.4; $C_{23}H_{19}N_5O_4V$ (480.37 g mol^{-1}) requires C, 57.51; H, 3.99; N, 14.58.

$K(H_2O)_2[V^VO_2(bp\text{-}bhz)]$ 5. Vanadium(v) oxide, V_2O_5 (0.18 g, 0.0010 mol), was suspended in an aqueous solution of KOH (0.11 g, 0.0020 mol in 5 mL H_2O) and stirred for 2 h with occasional heating at 50 °C. The resulting solution was then filtered. A filtered solution of **I** (0.67 g, 0.0020 mol), dissolved in 50 mL of aqueous KOH (0.22 g, 0.0040 mol), was added to the above solution. After 4 h of stirring the pH of the reaction mixture was slowly adjusted to *ca*. 7.5 with 4 M HCl. A yellowish-orange solid of **5** started to separate. The solution was filtered, and the solid was washed with cold methanol (2 × 5 mL) and dried in a desiccator over silica gel. Yield: 0.33 g (60%). Colour: yellow. Found: C, 52.2; H, 3.9; N, 10.4; $C_{24}H_{22}KN_4O_6V$ (552.49 g mol^{-1}) requires C, 52.17; H, 4.01; N, 10.14.

$K(H_2O)_2[V^VO_2(bp\text{-}fah)]$ 6. Complex **6** was prepared following the method outlined for **5** using ligand **II**. Yield: 0.37 g (68%). Colour: yellow. Found: C, 48.8; H, 3.7; N, 10.3; $C_{22}H_{20}KN_4O_7V$ (542.46 g mol^{-1}) requires C, 48.71; H, 3.72; N, 10.33.

$[V^VO_2(Hbp\text{-}bhz)]$ 7 and $[V^VO_2(Hbp\text{-}fah)]$ 8. Complexes **5** (0.53 g, 0.0010 mol) or **6** (0.52 g, 0.0010 mol) were dissolved in water (40 ml) and treated with aqueous HCl (1 mL of HCl diluted in 5 ml of water) with stirring until most of the complex had precipitated as a yellow solid. The solution was filtered, and the residue was washed with water and dried in a desiccator over silica gel.

7: Yield: 0.28 g (60%). Colour: yellow. Found: C, 60.5; H, 3.8; N, 11.9; $C_{24}H_{19}N_4O_4V$ (478.37 g mol^{-1}) requires C, 60.26; H, 4.00; N, 11.71.

8: Yield: 0.27 g (66%). Colour: yellow. Found: C, 56.6; H, 3.5; N, 11.8; $C_{22}H_{17}N_4O_5V$ (468.34 g mol^{-1}) requires C, 56.42; H, 3.66; N, 11.96.

$[V^VO_2(Hbp\text{-}nah)]$ 9 and $[V^VO_2(Hbp\text{-}inh)]$ 10. Vanadium(v) oxide, V_2O_5 (0.18 g, 0.0010 mol), was suspended in an aqueous solution of KOH (0.11 g, 0.0020 mol in 5 mL H_2O) and stirred for 1 h with occasional heating at 50 °C. The resulting solution was then filtered. A filtered solution of ligand H_2bp-nah **III** (0.79 g, 0.0020 mol) or H_2bp-inh **IV** (0.79 g, 0.0020 mol), dissolved in 50 mL of aqueous KOH (0.22 g, 0.0040 mol), was added to the above solution with stirring. The resulting reaction mixture was stirred for 4 h. After that, the pH of the reaction mixture was slowly adjusted to *ca*. 7.5 with 4 M HCl where orange solids of **9** or **10** slowly started to separate. After 1 h, the separated solids were filtered, washed with cold water (2 × 5 mL) and dried in a desiccator over silica gel.

9: Yield: 0.25 g (60%). Colour: yellow. Found: C, 57.7; H, 3.7; N, 14.8; $C_{23}H_{18}N_5O_4V$ (479.36 g mol^{-1}) requires C, 57.63; H, 3.78; N, 14.61.

10: Yield: 0.25 g (61%). Colour: yellow. Found: C, 51.2; H, 3.9; N, 16.6; $C_{23}H_{18}N_5O_4V$ (479.36 g mol^{-1}) requires C, 57.63; H, 3.78; N, 14.61.

$[V^VO(bp\text{-}bhz)(OMe)]$ 11. Complex **1** (0.48 g, 0.0010 mol) was dissolved in MeOH (25 mL) and allowed to stand in an open flask for slow evaporation/oxidation. Black crystals separated within a week. Yield: 0.38 g (77%). Found: C, 60.7; H, 4.4; N, 11.6; $C_{25}H_{21}N_4O_4V$ (492.40 g mol^{-1}) requires C, 60.98; H, 4.30; N, 11.38.

$[V^VO(bp\text{-}fah)(OMe)]$ 12, $[V^VO(bp\text{-}nah)(OMe)]$ 13 and $[V^VO(bp\text{-}inh)(OMe)]$ 14. These complexes were prepared similarly to **11** from the respective oxidovanadium(IV) **2–4** complexes.

12: Yield: 0.39 g (80%). Found: C, 57.5; H, 4.0; N, 11.6; $C_{23}H_{19}N_4O_5V$ (482.36 g mol^{-1}), requires C, 57.27; H, 3.97; N, 11.62.

13: Yield: 0.34 g (70%). (Found: C, 58.5; H, 3.8; N, 14.6; $C_{24}H_{20}N_5O_4V$ (493.39 g mol^{-1}), requires, C, 58.42; H, 4.09; N, 14.19).

14: Yield: 0.37 g (75%). (Found: C, 58.6; H, 3.9; N, 14.2; $C_{24}H_{20}N_5O_4V$ (493.39 g mol^{-1}), requires, C, 58.42; H, 4.09; N, 14.19).

Catalytic activity

Aromatization of Hantzsch 1,4-dihydropyridines

Benzaldehyde (0.53 g, 0.0050 mol), ethylacetoacetate (1.1 g, 0.010 mol) and ammonium acetate (0.38 g, 0.0050 mol) were mixed in a flask and, after adding the selected catalyst precursor (0.0010 g), the reaction mixture was stirred for 1 h at room temperature. The progress of the reaction was monitored by GC by withdrawing small aliquots of the reaction mixture, extracting with *n*-hexane and injecting into the GC column. The structures of the products were confirmed by GC-MS and by comparison with authentic samples reported in the literature.

Oxidation of tetralin

In a typical reaction, tetralin (1.3 g, 0.010 mol) and 30% H_2O_2 (2.3 g, 0.020 mol) were taken in 5 mL of CH_3CN and 0.0020 g of the complex was added. Then the reaction mixture was stirred at 80 °C for the desired time. The obtained reaction product was identified by GC analysis and confirmed by GC-MS.

X-Ray crystal structure determination

Three-dimensional X-ray data were collected on a Bruker Kappa Apex CCD diffractometer at low temperature for **5** and

7, and at room temperature for **6**, **8**, **9**, **10** and **12**, by the ϕ–ω scan method. Reflections were measured from a hemisphere of data collected from frames, each of them covering 0.3° in ω. A total of 38 439 reflections measured for **5**, 35 394 for **6**, 24 559 for **7**, 44 518 for **8**, 29 571 for **9**, 47 446 for **10** and 28 005 for **12** were corrected for Lorentz and polarization effects and for absorption by multi-scan methods based on symmetry-equivalent and repeated reflections. Of the total independent reflections, 4288 for **5**, 3365 for **6**, 2533 for **7**, 3381 for **8**, 3140 for **9**, 4556 for **10** and 3431 for **12** exceeded the significance level ($|F|/\sigma|F|$) > 4.0. After data collection, in each case a multi-scan absorption correction (SADABS)[37] was applied, and the structure was solved by direct methods and refined by full matrix least-squares on F^2 data using the SHELX suite of programs.[38] Hydrogen atoms were located in a difference Fourier map and left to refine freely in **5**, except for O(1W), which were located in a difference Fourier map and fixed to the oxygen atom. In **6** and **7** the hydrogen atoms were included in calculated positions and refined in the riding mode, except for the water molecules, which were located in a difference Fourier map, calculated and refined by the wingx program[39] and fixed on the oxygen atom. In **8** and **9** the hydrogen atoms were located in a difference Fourier map and left to refine freely, except for C(4), which were included in calculated positions and refined in the riding mode. In **10** the hydrogen atoms were located in a difference Fourier map and left to refine freely, except for C(1S), C(2S) and C(4), which were included in calculated positions and refined in the riding mode. In **12** the hydrogen atoms were located in a difference Fourier map and left to refine freely, except for C(1S), C(4) and C(20), which were included in calculated positions and refined in the riding mode. Refinements were done making allowance for thermal anisotropy of all non-hydrogen atoms. A final difference Fourier map showed no residual density outside: 0.425 and −0.654 e Å^{-3} for **5**, 0.617 and −0.772 e Å^{-3} for **6**, 1.182 and −0.429 e Å^{-3} for **7**, 0.370 and −0.406 e Å^{-3} for **8**, 0.501 and −0.507 e Å^{-3} for **9**, 0.676 and −0.382 e Å^{-3} for **10** and 0.272 and −0.380 e Å^{-3} for **12**. A weighting scheme, $w = 1/[\sigma^2(F_o^2) + (0.061000P)^2 + 0.708500P]$ for **5**, $w = 1/[\sigma^2(F_o^2) + (0.115500P)^2 + 0.00000P]$ for **6**, $w = 1/[\sigma^2(F_o^2) + (0.142000P)^2 + 0.000000P]$ for **7**, $w = 1/[\sigma^2(F_o^2) + (0.058700P)^2 + 3.998300P]$ for **8**, $w = 1/[\sigma^2(F_o^2) + (0.076200P)^2 + 0.00000P]$ for **9**, $w = 1/[\sigma^2(F_o^2) + (0.065700P)^2 + 0.371500P]$ for **10** and $w = 1/[\sigma^2(F_o^2) + (0.068700P)^2 + 3.405000P]$ for **12**, where $P = (|F_o|^2 + 2|F_c|^2)/3$, was used in the later stages of the refinement. Further details of the crystal structure determination are given in Table 1.

Results and discussion

Synthesis and characterization of the complexes

Scheme 2 depicts an overview of the complexes reported in this work. The structures of the complexes are based on elemental analyses, spectroscopic data (IR, UV/Vis, EPR, ^{1}H, ^{13}C and ^{51}V NMR), thermogravimetric studies and X-ray diffraction analyses of complexes **5–10** and **12**.

Reaction of $[V^{IV}O(acac)_2]$ with an equimolar amount of the ligands in methanol leads to the formation of the oxidovanadium(IV) complexes $[V^{IV}O(bp\text{-}bhz)(H_2O)]$ **1**, $[V^{IV}O(bp\text{-}fah)(H_2O)]$ **2**, $[V^{IV}O(bp\text{-}nah)(H_2O)]$ **3** and $[V^{IV}O(bp\text{-}inh)(H_2O)]$ **4** [eqn (1)]. All ligands coordinate to the metal ion in the dianionic [ONO^{2-}] enolate tautomeric form (see Scheme 2).

$$\begin{aligned} &2\left[V^{IV}O(acac)_2\right] + H_2L + H_2O \\ &\rightarrow \left[V^{IV}O(L)(H_2O)\right] + 2Hacac \\ &(H_2L = \text{ligands } \mathbf{I} - \mathbf{IV}) \end{aligned} \quad (1)$$

Aerial oxidation, along with prolonged crystallisation of these complexes in MeOH, results in the formation of $[V^{V}O(L)(OMe)]$ **11–14** [eqn (2) considering complex **1** as a representative].

$$\begin{aligned} &2\left[V^{IV}O(bp-bhz)(H_2O)\right] + \frac{1}{2}O_2 + 2\ MeOH \\ &\rightarrow 2\left[V^{V}O(bp-bhz)(OMe)\right] + 3H_2O \end{aligned} \quad (2)$$

Complexes $[K(H_2O)_2][V^{V}O_2(bp\text{-}bhz)]$ **5** and $[K(H_2O)_2][V^{V}O_2(bp\text{-}bhz)]$ **6** were isolated from the reaction of vanadate, prepared *in situ* by stirring V_2O_5 in aqueous KOH, with ligands **I** and **II**, respectively, while adjusting the pH to *ca.* 7 using HCl, eqn (3).

$$\begin{aligned} &K[H_2VO_4] + H_2L \\ &\rightarrow \left[K(H_2O)_2\right]\left[V^{V}O_2L\right]\ (H_2L = \mathbf{I}:\mathbf{5};\ H_2L = \mathbf{II}:\mathbf{6}) \end{aligned} \quad (3)$$

Due to the protonation of the pyridinic nitrogen, ligands **III** and **IV** gave complexes $[V^{V}O_2(Hbp\text{-}nah)]$ **9** and $[V^{V}O_2(Hbp\text{-}inh)]$ **10**, respectively, under similar reaction conditions, eqn (4).

$$\begin{aligned} &K[H_2VO_4] + H_2L + HCl \rightarrow \left[V^{V}O_2HL\right] \\ &+ KCl + 2H_2O\ (H_2L = \mathbf{III}:9;\ H_2L = \mathbf{IV}:\mathbf{10}) \end{aligned} \quad (4)$$

Similar complexes $[V^{V}O_2(Hbp\text{-}bhz)]$ **7** and $[V^{V}O_2(Hbp\text{-}fah)]$ **8**, where the ligands coordinate to the metal ion in the ketonic (hydrazide) form, were isolated upon the acidification of aqueous solutions of complexes **5** and **6**, respectively, with dilute HCl, eqn (5).

$$\begin{aligned} &\left[K(H_2O)_2\right]\left[V^{V}O_2L\right] + HCl \\ &\rightarrow \left[V^{V}O_2HL\right] + KCl + 2H_2O(H_2L = \mathbf{I}:7;\ H_2L = \mathbf{II}:\mathbf{8}) \end{aligned} \quad (5)$$

Structure descriptions

Several crystals suitable for X-ray diffraction studies were obtained and their structural features are analyzed below. Table 2 provides selected bond lengths and angles for all compounds. In all crystal structures, which were found for compounds **5–10** and **12**, the metal center is five coordinated and the geometry is best described as square pyramidal (see the discussion below).

Compounds **5** and **6** show a dimeric structure due to the presence of cation–π interactions between the neutral aromatic systems and K^+ ions, which control the assembly in dimeric aggregates. Fig. 1 and 2 depict ORTEP representations of the

Table 1 Crystal data and structure refinement for $[K(H_2O)_2\{V^VO_2(bp\text{-}bhz)\}]_2$ **5**, $[K(H_2O)_2\{V^VO_2(bp\text{-}fah)\}]_2$ **6**, $[V^VO_2(Hbp\text{-}bhz)]\cdot 1.5H_2O$ **7**·$1.5H_2O$, $[V^VO_2(Hbp\text{-}fah)]$ **8**, $[V^VO_2(Hbp\text{-}nah)]$ **9**, $[V^VO_2(Hbp\text{-}inh)]$·DMSO **10**·DMSO and $[V^VO(bp\text{-}fah)(OCH_3)]$ **12**

	5	**6**	**7**·$1.5H_2O$	**8**
Formula	$C_{48}H_{44}K_2N_8O_{12}V_2$	$C_{44}H_{40}K_2N_8O_{14}V_2$	$C_{24}H_{22}N_4O_{5.50}V$	$C_{22}H_{17}N_4O_5V$
Formula weight	1104.99	1084.90	505.40	468.34
T, K	100(2)	293(2)	100(2)	293(2)
Wavelength, Å	0.71073	0.71073	0.71073	0.71073
Crystal system	Triclinic	Monoclinic	Triclinic	Monoclinic
Space group	$P\bar{1}$	$P2_1/c$	$P\bar{1}$	$C2/c$
a/Å	8.5326(3)	11.6725(8)	8.5590(16)	25.862(3)
b/Å	10.2707(3)	22.2312(15)	10.2574(18)	7.1899(7)
c/Å	14.0922(5)	9.1846(6)	14.448(2)	21.357(2)
α/°	87.943(2)		83.719(11)	
β/°	82.422(2)	96.914(2)	78.317(11)	98.156(5)
γ/°	70.9430(10)		71.534(11)	
V/Å^3	1157.07(7)	2366.0(3)	1176.8(4)	3931.0(7)
Z	1	2	2	8
F_{000}	568	1108	522	1920
$D_{calc.}$/g cm^{-3}	1.586	1.520	1.426	1.583
μ/mm^{-1}	0.659	0.646	0.467	0.550
θ/°	1.46 to 26.39	1.76 to 28.62	1.44 to 26.43	1.59 to 26.38
R_{int}	0.0336	0.0515	0.0706	0.0474
Crystal size/mm^3	0.41 × 0.25 × 0.20	0.31 × 0.29 × 0.13	0.16 × 0.11 × 0.08	0.16 × 0.14 × 0.13
Goodness-of-fit on F^2	1.132	1.024	1.012	1.107
$R_1[I > 2\sigma(I)]^a$	0.0313	0.0595	0.0705	0.0315
wR_2 (all data)^b	0.1074	0.1961	0.2421	0.1040
Largest differences between peak and hole (e Å^{-3})	0.425 and −0.654	0.617 and −0.772	1.186 and −0.437	0.370 and −0.406

	9	**10**·DMSO	**12**
Formula	$C_{23}H_{18}N_5O_4V$	$C_{25}H_{24}N_5O_5SV$	$C_{23}H_{19}N_4O_5V$
Formula weight	479.36	557.49	482.36
T, K	293(2)	293(2)	293(2)
Wavelength, Å	0.71073	0.71073	0.71073
Crystal system	Triclinic	Triclinic	Monoclinic
Space group	$P\bar{1}$	$P\bar{1}$	$C2/c$
a/Å	9.0595(8)	8.2826(7)	14.133(4)
b/Å	9.6948(9)	11.0071(9)	11.772(4)
c/Å	12.4414(13)	14.2227(12)	26.621(8)
α/°	95.526(6)	87.501(5)	
β/°	98.606(6)	81.094(5)	103.350(17)
γ/°	94.410(6)	82.501(4)	
V/Å^3	1070.77(18)	1269.69(18)	4309(2)
Z	2	2	8
F_{000}	492	576	1984
$D_{calc.}$/g cm^{-3}	1.487	1.458	1.487
μ/mm^{-1}	0.505	0.519	0.504
θ/°	1.67 to 26.41	1.45 to 26.42	1.57 to 28.43
R_{int}	0.0711	0.0378	0.0431
Crystal size/mm^3	0.22 × 0.13 × 0.06	0.49 × 0.17 × 0.12	0.32 × 0.20 × 0.16
Goodness-of-fit on F^2	1.055	1.109	1.060
$R_1[I > 2\sigma(I)]^a$	0.0457	0.0331	0.0495
wR_2 (all data)^b	0.1318	0.1128	0.1476
Largest differences between peak and hole (e Å^{-3})	0.501 and −0.507	0.676 and −0.382	0.272 and −0.380

$^a R_1 = \sum||F_o| - |F_c||/\sum|F_o|$. $^b wR_2 = \{\sum[w(||F_o|^2 - |F_c|^2|)^2]|/\sum[w(F_o^2)^2]\}^{1/2}$.

asymmetric units, while Fig. 3 and 4 show the dimeric aggregates. In both crystal structures the metal centers are coordinated by one terminal oxygen atom [V(1)–O(1), 1.6264(15) Å in **5** and 1.605(2) Å in **6**], one bridging oxygen atom with the K^+ ion [V(1)–O(2), 1.6386(15) Å in **5** and 1.639(2) Å in **6**], two oxygen atoms of the ligands (bp-bhz in **5** and bp-fah in **6**) [V(1)–O(3), 1.9185(14) Å in **5** and 1.936(2) Å in **6** and V(1)–O(4), 1.9634(15) Å in **5** and 1.968(2) Å in **6**] and one nitrogen atom of the azomethine group [V(1)–N(1), 2.1672(16) Å in **5** and 2.190(3) Å in **6**]. The geometric parameter $\tau = (\beta - \alpha)/60$, where β and α are the two largest L–M–L angles, can be used to describe the polyhedron defined by five coordinated atoms. It has a value of 1 if the structure is pentagonal bipyramidal and 0 if it is square pyramidal. For **5** ($\alpha_{O2\text{–}V1\text{–}N1}$ = 146.55°, $\beta_{O3\text{–}V1\text{–}O4}$ = 147.53°) and **6** ($\alpha_{O2\text{–}V1\text{–}N1}$ = 146.04°, $\beta_{O3\text{–}V1\text{–}O4}$ = 145.74°) the τ values of 0.02 and 0.01, respectively, indicate a square pyramidal geometry.[40] Nevertheless, they are not isostructural compounds around the K^+ ions. In **5** the alkali metal coordinates to the π-face of the phenyl group of the ligand (bp-bhz) [mean of the distances to carbon atoms, 3.325(2) Å], two water mole-

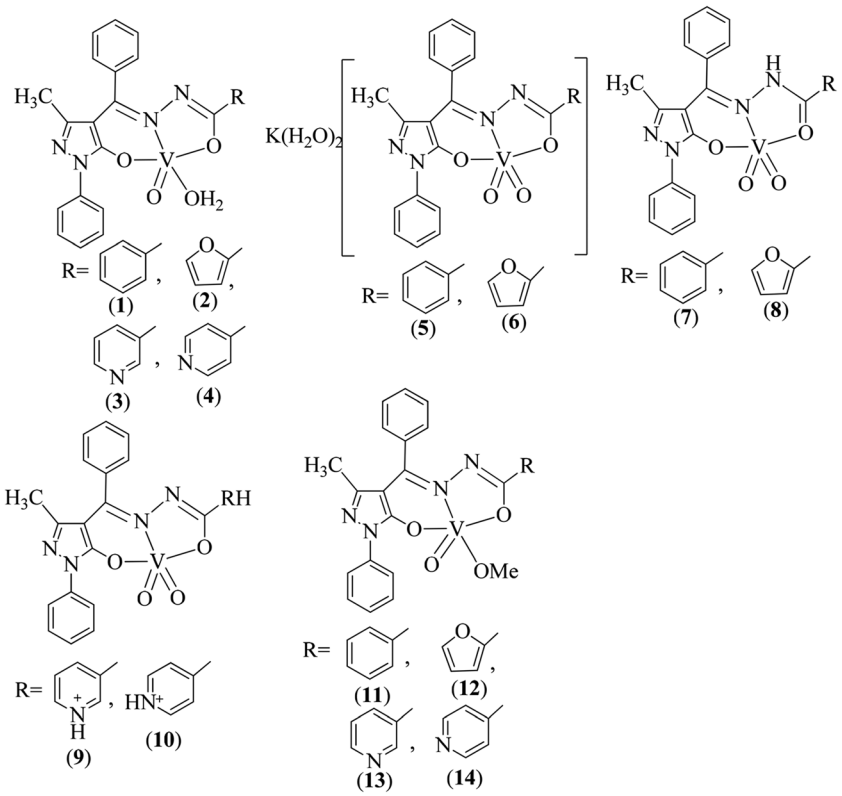

Scheme 2 Proposed structures for the complexes reported in this work.

cules [K(1)–O(1W), 2.827(2) Å and K(1)–O(2W) 2.7739(18) Å], two oxygen bridging atoms which present an important asymmetry, one of them being the oxygen atom of the oxido groups [V(1)–O(2), 1.6386(15) Å and K(1)–O(2), 2.7576(16) Å] and the other the oxygen atom of the hydrazide group [V(1)–O(4), 1.9634(15) Å and K(1)–O(4), 3.2355(16) Å], one M–$N_{azomethine}$ dative bond [K(1)–N(2), 2.8736(17) Å] and one lateral η^1-cation–π interaction with a carbon atom [distance K(1)–C(14), 3.188(2) Å] of the other phenyl group. In **6**, the K^+ ion coordinates to the π-face of the phenyl group of the ligand (bp-fah) [mean of the distances to carbon atoms, 3.341(2) Å], two water molecules (one of them presenting a disorder) [K(1)–O(1W), 2.844(4) Å and K(1)–O(2WA), 2.693(8) Å and K(1)–O(2WB), 2.83(2) Å], one oxido group [V(1)–O(2), 1.639(2) Å and K(1)–O(2), 2.781(3) Å] and one enolic oxygen atom of the pyrazolone group [V(1)–O(3), 1.936(2) Å and K(1)–O(3), 3.256(2) Å], one M–$N_{azomethine}$ dative bond [K(1)–N(2), 2.914(3) Å] and one oxygen atom of the furan ring [K(1)–O(5), 2.706(2) Å]. The distances K–$Ph_{centroid}$ are 3.022(2) Å in **5** and 3.042(2) Å in **6**, similar to those found in other compounds with the same type of cation–π interactions.[41]

The pyrazol group (C1, C2, C3, N3, N4) and the phenyl of the hydrazide group (C13, C14, C15, C16, C17, C18) are not coplanar in **5** [mean deviation from planarity, 0.1386(17) Å]. In **6**, the furan ring of the hydrazide group (C19, C20, C21, C22, O5) and the pyrazolone group (C1, C2, C3, N3, N4) are coplanar [mean deviation from planarity, 0.0679(25) Å], and the other phenyl group (C12, C13, C14, C15, C16, C17) forms a torsion angle of 25.78(14)°, over the previous coplanar groups. In **5**, the vanadium atom is displaced toward the apical oxido ligand (O1) from the equatorial plane defined by O2, O3, O4 and N1 atoms, 0.4979(7) Å [mean deviation from planarity, O2, O3, O4, N1, 0.0034(8) Å]. In **6**, the displacement is 0.5228(11) Å [mean deviation from planarity, O2, O3, O4, N1, 0.0174(12) Å]. The two apical oxygen atoms present V=O bonds characteristic of oxido-type O atoms with strong π bonding.[42,43] The V–K separations depend on the position of the K^+ ion in the dimeric aggregates and are 3.8532(6) Å in **5** and 3.7644(11) Å in **6**.

In addition, π–π interactions, hydrogen bonding and electrostatic interactions are present in the crystal structures of compounds **5** and **6**. This results in different crystal packings in the two compounds. In **5** there are π–π interactions between dimeric aggregates (see Fig. S1†) through face-to-face motifs [distance between centroids of phenyl rings bonded to the pyrazolone group, d_{c1-c2}, 3.569(8) Å [c1(C19H, C20H, C21H, C22H, C23H, C24H) and c2(C19T, C20T, C21T, C22T, C23T, C24T)], and edge-to-face motifs between phenyl groups $d_{C11s-c3}$, 3.502(9) Å [c3(C13J, C14J, C15J, C16J, C17J, C18J)]. In **6** the dimeric aggregates are placed differently in the crystal packing, due to the absence of π–π interactions, the hydrogen bonds (see Table 2) being the predominant interaction (see Fig. S2†).

Compounds **7**, **8**, **9** and **10** contain vanadium mononuclear complexes with ligands bp-bhz, bp-fah, bp-nah and bp-inh,

Table 2 Bond lengths (Å) and angles (°) for the compounds $[K(H_2O)_2\{V^VO_2(bp\text{-}bhz)\}]_2$ **5**, $[K(H_2O)_2\{V^VO_2(bp\text{-}fah)\}]_2$ **6**, $[V^VO_2(Hbp\text{-}bhz)]\cdot 1.5H_2O$ **7**·$1.5H_2O$, $[V^VO_2(Hbp\text{-}fah)]$ **8**, $[V^VO_2(Hbp\text{-}nah)]$ **9**, $[V^VO_2(Hbp\text{-}inh)]$·DMSO **10**·DMSO and $[V^VO(bp\text{-}fah)(OMe)]$ **12**

Bond lengths	5	6	7·1.5H_2O	8
V(1)–O(1)	1.6264(15)	1.605(2)	1.594(3)	1.6265(14)
V(1)–O(2)	1.6386(15)	1.639(2)	1.612(3)	1.6143(14)
V(1)–O(3)	1.9185(14)	1.936(2)	1.914(3)	1.9387(13)
V(1)–O(4)	1.9634(15)	1.968(2)	1.993(3)	2.0255(14)
V(1)–N(1)	2.1672(16)	2.190(3)	2.169(4)	2.1958(16)
V(1)–K(1)	3.8532(6)	3.7644(11) #2		
K(1)–O(2)	2.7576(16)	2.781(3) #2		
K(1)–O(3)		3.255(2) #2		
K(1)–O(4)	3.2355(16)			
K(1)–O(5)		2.706(2)		
K(1)–O(2W)	2.7739(18)			
K(1)–O(2WA)		2.693(8)		
K(1)–O(2WB)		2.889(18) #2		
K(1)–O(1W)	2.827(2)	2.844(4) #3		
K(1)–N(2)	2.8736(17) #1	2.915(3)		
K(1)–C(6)	3.257(2) #1	3.313(3)		
K(1)–C(7)	3.200(2) #1	3.346(3)		
K(1)–C(8)	3.239(2) #1	3.376(4)		
K(1)–C(9)	3.381(2) #1	3.351(4)		
K(1)–C(10)	3.476(2) #1	3.330(4)		
K(1)–C(11)	3.396(2) #1	3.330(3)		
K(1)–C(14)	3.188(2) #1			

Bond lengths	9	10·DMSO	12
V(1)–O(1)	1.618(2)	1.6156(15)	1.573(2)
V(1)–O(2)	1.6317(19)	1.6238(13)	1.761(2)
V(1)–O(3)	1.9404(18)	1.9460(14)	1.8727(19)
V(1)–O(4)	1.9514(19)	1.9666(14)	1.8840(19)
V(1)–N(1)	2.172(2)	2.1789(15)	2.104(2)

Angles	5	6	7·1.5H_2O	8
O(1)–V(1)–O(2)	107.95(8)	107.95(13)	108.6(2)	108.92(7)
O(1)–V(1)–O(3)	105.78(7)	104.66(11)	104.09(16)	102.27(6)
O(2)–V(1)–O(3)	95.76(7)	92.27(11)	96.17(16)	96.62(7)
O(1)–V(1)–O(4)	103.69(7)	105.70(12)	101.42(17)	97.05(6)
O(2)–V(1)–O(4)	89.89(7)	93.11(10)	90.88(15)	94.24(6)
O(3)–V(1)–O(4)	146.55(6)	145.76(10)	149.71(14)	153.35(6)
O(1)–V(1)–N(1)	103.09(7)	105.70(12)	107.93(16)	108.56(6)
O(2)–V(1)–N(1)	147.53(7)	146.04(11)	142.41(17)	141.83(7)
O(3)–V(1)–N(1)	84.62(6)	83.55(9)	83.12(13)	82.27(6)
O(4)–V(1)–N(1)	73.54(6)	73.35(9)	73.63(13)	74.23(5)
O(1)–V(1)–K(1)	130.01(6)	138.23(9) #2		
O(2)–V(1)–K(1)	38.17(5)	42.31(9) #2		
O(3)–V(1)–K(1)	111.79(4)	59.85(7) #2		
O(4)–V(1)–K(1)	57.03(4)	104.62(7) #2		
N(1)–V(1)–K(1)	111.97(4)	110.07(7) #2		

Angles	9	10·DMSO	12
O(1)–V(1)–O(2)	110.05(10)	108.07(8)	107.31(12)
O(1)–V(1)–O(3)	104.20(9)	104.92(8)	106.09(11)
O(2)–V(1)–O(3)	93.23(9)	94.54(7)	91.39(9)
O(1)–V(1)–O(4)	102.38(9)	103.88(8)	106.79(11)
O(2)–V(1)–O(4)	93.13(9)	92.42(6)	92.17(9)
O(3)–V(1)–O(4)	148.60(8)	146.53(6)	144.17(9)
O(1)–V(1)–N(1)	104.50(9)	103.69(7)	99.78(10)
O(2)–V(1)–N(1)	145.05(10)	147.59(7)	152.49(10)
O(3)–V(1)–N(1)	83.12(8)	83.28(6)	85.58(8)
O(4)–V(1)–N(1)	74.24(8)	73.63(6)	75.19(8)

Symmetry transformations used to generate equivalent atoms: #1 $-x+1, -y+1, -z$ #2 $-x+1, -y, -z+1$ #3 $-x+1, -y, -z$.

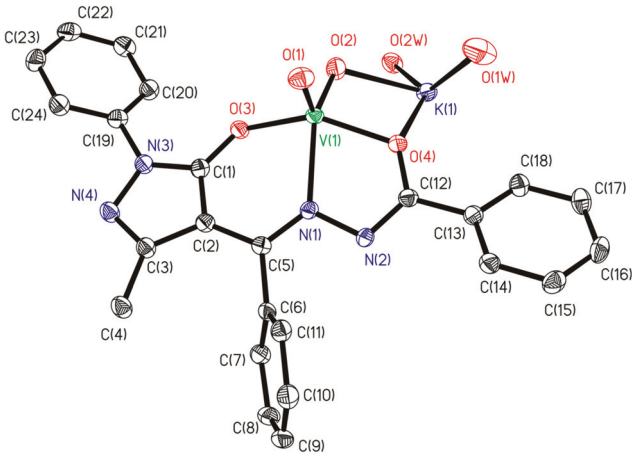

Fig. 1 ORTEP plot of the asymmetric unit of compound $[K(H_2O)_2\{V^VO_2(bp\text{-}bhz)\}]_2$ **5**. All the non-hydrogen atoms are presented by their 50% probability ellipsoids. Hydrogen atoms are omitted for clarity.

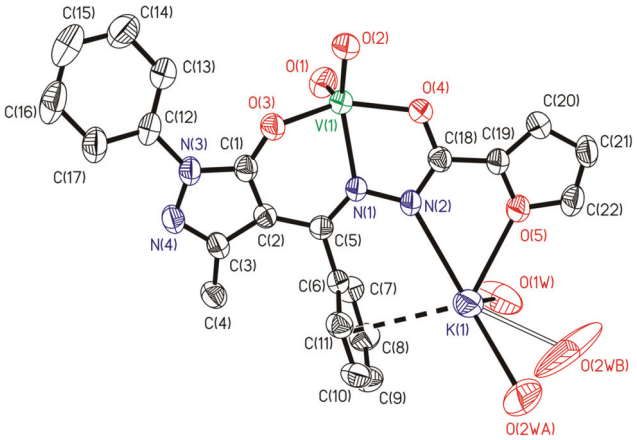

Fig. 2 ORTEP plot of the asymmetric unit of compound $[K(H_2O)_2\{V^VO_2(bp\text{-}fah)\}]_2$ **6**. All the non-hydrogen atoms are presented by their 50% probability ellipsoids. Hydrogen atoms are omitted for clarity.

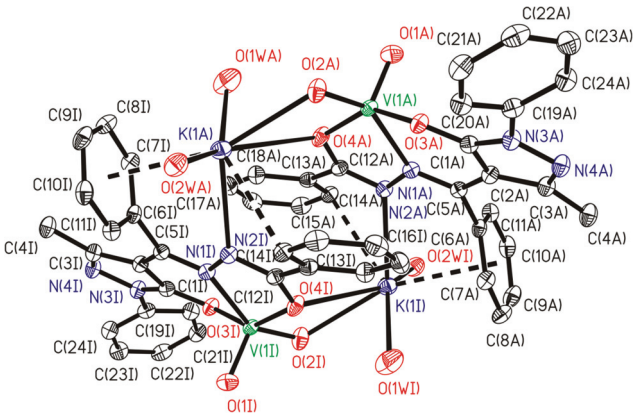

Fig. 3 Dimeric aggregate in the compound $[K(H_2O)_2\{V^VO_2(bp\text{-}bhz)\}]_2$ **5**. Dashed black lines show π-face and lateral η^1-cation–π interactions of K^+ ions and phenyl groups. All the non-hydrogen atoms are presented by their 50% probability ellipsoids. Hydrogen atoms are omitted for clarity.

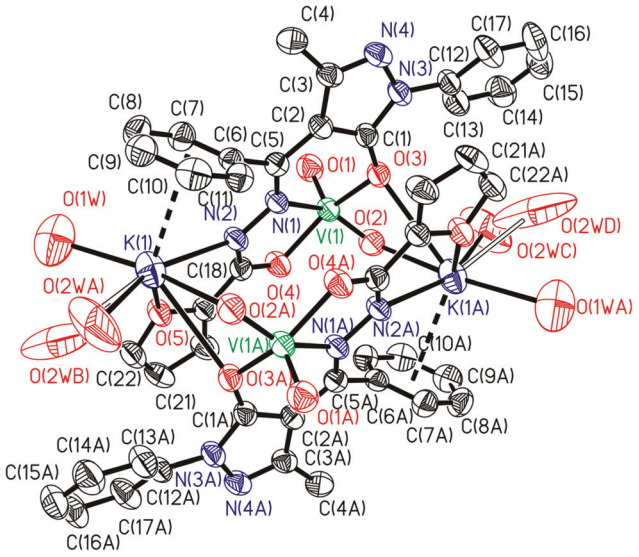

Fig. 4 Dimeric aggregate in the compound $[K(H_2O)_2\{V^VO_2(bp\text{-}fah)\}]_2$ **6**. All the non-hydrogen atoms are presented by their 50% probability ellipsoids. Hydrogen atoms are omitted for clarity.

respectively, which are all protonated. The ligands bp-bhz and bp-fah are protonated at the azomethine nitrogen atom, N(2), and the ligands bp-nah and bp-inh at the nitrogen atom of the pyridine ring. Fig. 5–8 show ORTEP representations of the complexes in the asymmetric units. For **7** ($\alpha_{O3\text{–}V1\text{–}O4}$ = 149.69°, $\beta_{O2\text{–}V1\text{–}N1}$ = 142.36°), **8** ($\alpha_{O3\text{–}V1\text{–}O4}$ = 153.35°, $\beta_{O2\text{–}V1\text{–}N1}$ = 141.83°), **9** ($\alpha_{O3\text{–}V1\text{–}O4}$ = 148.60°, $\beta_{O2\text{–}V1\text{–}N1}$ = 145.05°) and **10** ($\alpha_{O3\text{–}V1\text{–}O4}$ = 146.53(6)°, $\beta_{O2\text{–}V1\text{–}N1}$ = 147.59(7)°), the calculated τ values of 0.122, 0.192, 0.059 and 0.018, respectively, indicate a distorted square pyramidal geometry.[40]

The pyrazol group (C1, C2, C3, N3, N4) and the phenyl, furan and pyridine rings of the hydrazide groups (C13, C14, C15, C16, C17, C18 in **7**; C19, C20, C21, C22, O5 in **8**; C13,

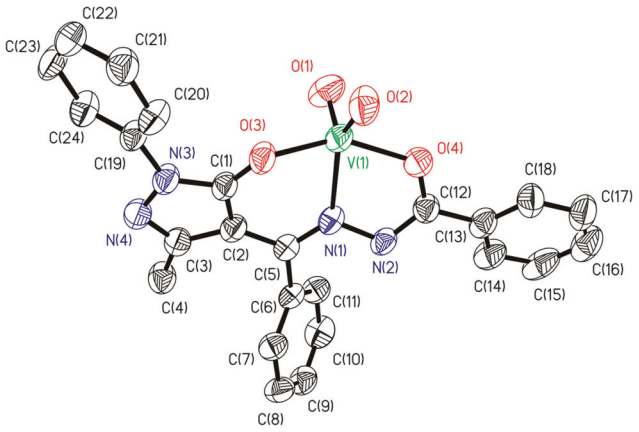

Fig. 5 ORTEP plot of the vanadium complex in $[V^VO_2(Hbp\text{-}bhz)]\cdot 1.5H_2O$ **7**·1.5H_2O. All the non-hydrogen atoms are presented by their 50% probability ellipsoids. Hydrogen atoms and water molecules are omitted for clarity.

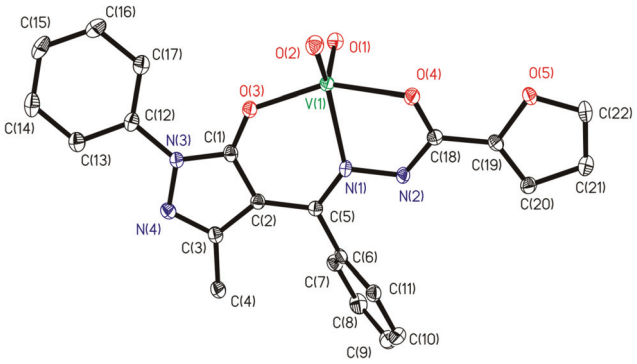

Fig. 6 ORTEP plot of $[V^VO_2(Hbp\text{-}fah)]$ **8**. All the non-hydrogen atoms are presented by their 50% probability ellipsoids. Hydrogen atoms are omitted for clarity.

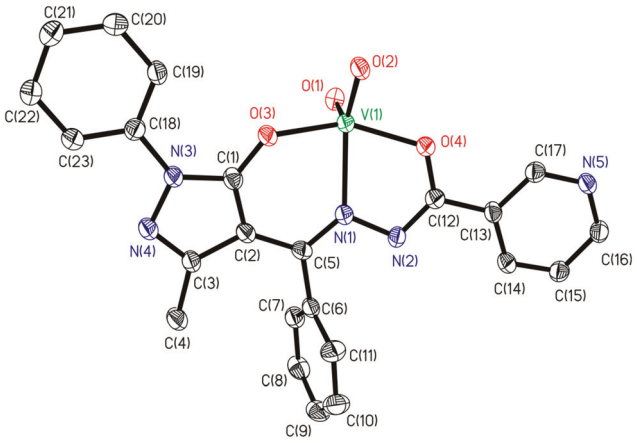

Fig. 7 ORTEP plot of $[V^VO_2(Hbp\text{-}nah)]$ **9**. All the non-hydrogen atoms are presented by their 50% probability ellipsoids. Hydrogen atoms are omitted for clarity.

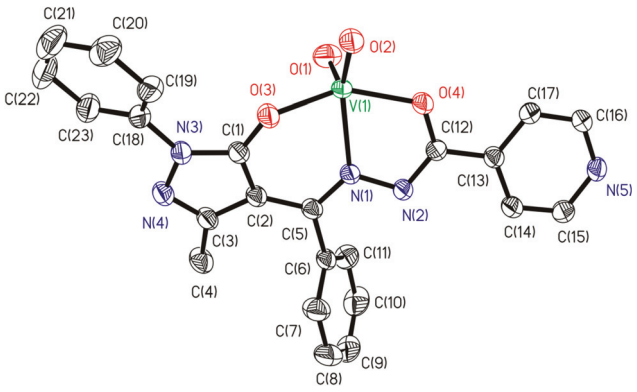

Fig. 8 ORTEP plot of vanadium complex in $[V^VO_2(Hbp\text{-}inh)]\cdot DMSO$ **10**·DMSO. All the non-hydrogen atoms are presented by their 50% probability ellipsoids. Hydrogen atoms and the DMSO molecule are omitted for clarity.

C14, C15, C16, C17, N5 in **9** and C13, C14, C15, C16, C17, N5 in **10**) are coplanar in **7**, **8** and **9** [mean deviation from planarity, 0.0923(39) Å, 0.0386(16) Å and 0.0372(22) Å, respectively] and not coplanar in **10** [mean deviation from planarity, 0.2078(17) Å]. Again, the vanadium atoms in complexes **7**, **8**, **9** and **10** are displaced towards the apical oxido ligand (O1) from the equatorial plane defined by O2, O3, O4 and N1 atoms, 0.5011(7) Å, 0.4591(8) Å, 0.5011(10) Å and 0.4975(7) Å [mean deviation from planarity, O2, O3, O4, N1, 0.0819(18) Å, 0.1425(7) Å, 0.0529(10) Å and 0.0120(8) Å], respectively. The two apical oxygen atoms present V=O bonds characteristic of oxido-type O atoms with strong π bonding.

In Fig. S3–S6† the crystal packing of compounds **7**–**10** is depicted. For complex **7** it can be described as layers of vanadium complexes interacting by van der Waals forces. Water molecules are placed between layers in a network of hydrogen bonds (see Table 2). The crystal packing of compound **8** presents dimeric aggregates, which interact by hydrogen bonds. In **9** the crystal packing also presents layers; however the interaction between layers is through π–π stacking between delocalized π-clouds around the N–N azomethine bond and pyridine rings, d_{c4-c5}, 3.385(10) Å, [c4(N3D–N4D) and c5(C13C, C14C, C15C, C16C, C17C, N5C)], and also by hydrogen bonds (see Fig. S5†). The crystal packing of complex **10** is also in layers of vanadium complexes and DMSO molecules interacting through van der Waals forces (see Fig. S6†).

The crystal structure of compound **12** contains an oxidomethoxidovanadium(v) mononuclear complex with the ligand bp-fah. Fig. 9 shows the ORTEP drawing of the complex present in the asymmetric unit. For this complex the τ value of 0.192 [$\alpha_{O3-V1-O4}$ = 144.17(9)° and $\beta_{O2-V1-N1}$ = 152.49(10)°] suggests a distorted square pyramidal geometry.[40]

The pyrazol group (C1, C2, C3, N3, N4) and the furan ring of the hydrazide group (C19, C20, C21, C22, O5) are coplanar [mean deviation from planarity, 0.0700(23) Å]. The vanadium atom is displaced towards the apical oxido ligand (O1) from the equatorial plane defined by O2, O3, O4 and N1 atoms by 0.4947(10) Å [mean deviation from planarity, O2, O3, O4, N1, 0.0464(11) Å]. The apical oxygen atom presents a V=O bond characteristic of oxido-type O atoms with strong π bonding. In Fig. S7† the crystal packing of compound **12** is shown. The complexes are placed in layers, which interact by van der Waals forces (Table 3).

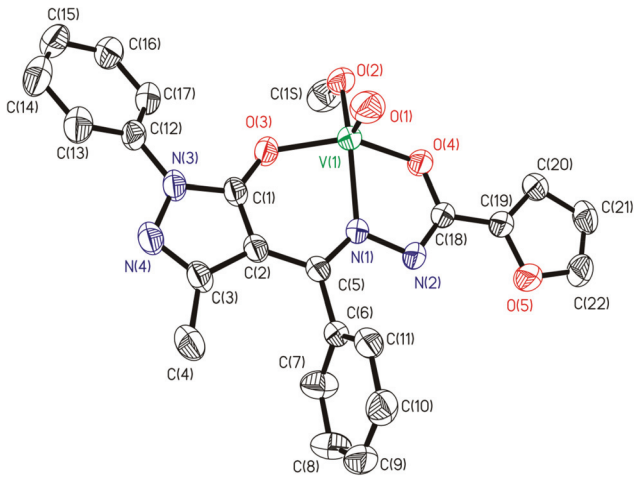

Fig. 9 ORTEP plot of [V^{V}O(Hbp-fah)(OMe)] **12**. All the non-hydrogen atoms are presented by their 50% probability ellipsoids. Hydrogen atoms are omitted for clarity.

Thermal analysis

Thermogravimetric analysis of the complexes was carried out under an oxygen atmosphere and relevant data are presented in Table S1.† All complexes are stable up to *ca.* 110 °C and thereafter they decompose exothermically in a few steps. Quantitative measurement of weight loss at different stages was not possible due to their overlap. Complexes **1**–**4** lose mass roughly equal to one H_2O molecule above 110 °C, indicating the presence of weakly coordinated H_2O to the metal center. Upon further increment of the temperature, the complexes decompose in three overlapping steps giving V_2O_5 as the final product at *ca.* 500 °C. Complexes **5** and **6** lose mass at *ca.* 130 °C, which is assigned to two water molecules that we attribute to the water molecules associated with the K ions. The water-free species decomposes in multiple exothermic but overlapping steps on further increasing the temperature, which are complete at *ca.* 600 °C to give KVO_3 as the final product. Complexes **7**–**10** are stable up to *ca.* 580 °C and

Table 3 Hydrogen bonds in the compounds $[K(H_2O)_2\{V^{V}O_2(bp\text{-}bhz)\}]_2$ **5**, $[K(H_2O)_2\{V^{V}O_2(bp\text{-}fah)\}]_2$ **6**, $[V^{V}O_2(Hbp\text{-}bhz)]\cdot 1.5H_2O$ **7**·$1.5H_2O$, $[V^{V}O_2(Hbp\text{-}fah)]$ **8**, $[V^{V}O_2(Hbp\text{-}nah)]$ **9** and $[V^{V}O_2(Hbp\text{-}inh)]$·DMSO **10**·DMSO

D–H···A (compound)	*d*(D–H)	*d*(H···A)	*d*(D···A)	<(DHA)
O(1W)–H(1WB)···O(1)#1 (**5**)	1.01	1.85	2.785(3)	151.7
O(1W)–H(1WB)···O(2)#1 (**5**)	1.01	2.57	3.381(3)	136.8
O(1W)–H(1WA)···O(4) (**5**)	1.07	2.00	2.800(2)	128.6
O(2W)–H(2WA)···O(1)#2 (**5**)	0.80(3)	2.11(3)	2.914(2)	176(3)
O(2W)–H(2WB)···O(2)#3 (**5**)	0.84(4)	2.24(4)	3.010(2)	152(3)
O(1W)–H(1WA)···O(4) (**6**)	0.85	2.15	2.998(4)	173.6
O(1W)–H(1WB)···O(2WB)#4 (**6**)	0.85	2.13	2.983(13)	176.0
O(2WA)–H(2WA)···O(1W)#5 (**6**)	0.85	2.29	2.879(10)	126.5
O(2WA)–H(2WA)···O(2)#5 (**6**)	0.85	2.57	3.000(9)	112.6
O(2WA)–H(2WB)···O(2)#6 (**6**)	0.85	2.31	3.156(8)	173.1
O(2WB)–H(2WD)···O(2)#7 (**6**)	0.85	2.24	2.790(11)	122.5
O(1W)–H(1WB)···O(2W) (7)	0.85	2.39	2.839(15)	113.3
O(1W)–H(1WA)···O(2)#8 (7)	0.85	1.91	2.757(5)	175.6
N(2)–H(2N)···O(1W) (7)	0.88	1.98	2.770(5)	148.8
O(2W)–H(2WB)···O(1W) (7)	0.84	2.00	2.839(15)	177.8
O(2W)–H(2WA)···O(1)#9 (7)	0.85	2.43	3.284(16)	175.7
O(3W)–H(3WB)···O(1W) (7)	0.86	2.10	2.957(12)	177.3
O(3W)–H(3WA)···O(1)#9 (7)	0.85	2.28	3.130(11)	176.8
N(2)–H(2N)···O(1)#10 (**8**)	0.84(3)	1.99(3)	2.770(2)	153(2)
N(5)–H(5N)···O(2)#11 (**9**)	1.02(3)	1.65(3)	2.612(3)	155(3)
N(5)–H(5N)···O(7)#12 (**10**)	0.82(3)	1.84(3)	2.661(2)	178(3)
N(5)–H(5N)···S(1)#12 (**10**)	0.82(3)	2.94(3)	3.6899(18)	153(2)

Symmetry transformations used to generate equivalent atoms: #1 $-x+1, -y, -z$ #2 $-x+1, y, z$ #3 $-x+2, -y, -z$ #4 $x, y, z-1$ #5 $-x+1, y-1/2, -z+1/2$ #6 $-x+1, -y, -z+1$ #7 $x, -y+1/2, z+1/2$ #8 $-x, -y+1, -z+1$ #9 2 $x, y-1, z$ #10 $-x, -y, -z$ #11 $-x+1, -y+1, -z+1$ #12 $x+1, y, z$.

beyond this temperature they decompose exothermically to give V_2O_5 as the final product. Complexes **11–14** undergo mass loss roughly equivalent to one methoxide (–OMe) group in the temperature range 120–160 °C, indicating the presence of one coordinated –OMe group. These complexes finally decompose giving the final product V_2O_5 in the temperature range 480–510 °C.

IR spectral studies

The IR spectral bands for ligands and complexes are presented in Table S2.† Comparison of the spectra of the complexes and the corresponding ligands elucidates the coordination mode of the ligands. The ketonic nature of the ligands in the solid state is indicated by the presence of ν(NH) and ν(C═O$_{\text{hydrazide/pyrazolone}}$) stretches at 3060–3130 and 1632–1647/1587–1594 cm^{-1}. Disappearance of these bands in the spectra of the complexes (except for **7** and **8**) indicates the enolization of the ketonic group and replacement of the H atom by the metal ion. A sharp band appearing in the region 1242–1265 cm^{-1} is assigned to the ν(C–O$_{\text{enolic}}$) mode. The sharp band at 1531–1542 cm^{-1} due to ν(C═N) (azomethine), in the ligands' spectra, shifts to lower wavenumbers in the complexes' spectra, appearing at 1520–1528 cm^{-1}, indicating the coordination of the azomethine nitrogen to the metal center. This is further supported by the shift of the ν(N–N), which appears at 1005–1011 cm^{-1} in the ligands and at 1044–1089 cm^{-1} in the complexes. The shift of the ν(N–N) band to higher frequency is expected because of the reduced repulsion between the lone pairs of adjacent nitrogen atoms. All ligands exhibit a broad band at *ca.* 3000 cm^{-1} due to the involvement of –OH groups in intramolecular hydrogen bonding. The presence of this band at 3380–3430 cm^{-1} in the complexes' spectra is possibly due to the breaking of hydrogen bonding as well as coordination of water (in complexes **1–6**). An additional band at 3066–3091 cm^{-1} in complexes **7–10** indicates the presence of the hydrazinic proton (in **7** and **8**) or protonated pyridinic nitrogen (in **9** and **10**).

A sharp band at 979–996 cm^{-1} (in the $V^{IV}O$ complexes **1–4**) and at 968–983 cm^{-1} (in $V^{V}O$ complexes **11–14**) is characteristic of the ν(V═O) stretch. The $V^{V}O_2$-complexes exhibit two sharp bands in the 899–943 cm^{-1} region due to ν_{sym}(O═V═O) and ν_{asym}(O═V═O) modes.

UV-vis spectral studies

A list of UV-vis spectral data of ligands and complexes is presented in Table S3.† Fig. 10 depicts UV-vis spectra of all complexes. Detailed spectral studies of ligands, **I–IV**, and their dioxidomolybdenum(VI) complexes have recently been reported by us.[35] The ligands exhibit three absorption bands at 204–205, 250–253 and 346–365 nm due to $\varphi \rightarrow \varphi^*$, $\pi \rightarrow \pi^*$ and $n \rightarrow \pi^*$ transitions, respectively. All these bands are also observed in the complexes' spectra but slightly shifted, indicating rearrangement of the ligand upon coordination to the metal ion. In addition, a new band of medium intensity appears at *ca.* 395–405 nm, which is assigned to a ligand to the metal charge transfer (LMCT) band, doubtlessly arising due to the transfer of electron density from the filled p-orbital of coordinated oxygen atoms to a vacant d-orbital of vanadium. At higher concentrations, two weak bands centered at 480–510 (shoulder) and 650–680 nm in the oxidovanadium(IV) complexes' spectra are observed and assigned to d–d transitions.

^{1}H NMR spectral study

Further evidence for the coordination mode of the ligands in the vanadium(V) complexes was established by NMR spectroscopy. ^{1}H NMR spectra of ligands **I–IV** and their $V^{V}O/V^{V}O_2$-complexes were recorded in [DMSO]-d_6 and the relevant spectral data are collected in Table 4 and representative spectra of H_2bp-fah **II**, $K(H_2O)_2[V^{V}O_2$(bp-fah)] **6**, [$V^{V}O_2$(Hbp-fah)] **8** and [$V^{V}O$(bp-fah)(OMe)] **12** are presented in Fig. 11. They give further support to the assignments made by IR and UV-vis absorption spectroscopy. In the ligands' spectra the signal appearing at δ = 10.96–11.46 ppm due to the NH proton and at δ = 1.45–1.48 ppm due to the ring proton of the pyrazole residue indicate the ketonic form of both C═O groups in solution. The absence of these signals in complexes **5**, **6**, **11–14** corroborates the enolisation and subsequent substitution of the proton by the metal ion. The neutral complexes **7** and **8** exhibit the –NH resonance at nearly the same chemical shift possibly due to protonation of the hydrazido nitrogen (see the description of the crystal structures) to compensate for the charge. In complexes **9** and **10** such a resonance could not be located. Protons due to the methyl group appear at 1.38–1.46 ppm in both the ligands' and complexes' spectra. Aromatic protons appear in the expected region with slight shifts in their positions in the complexes' spectra. Coordination of methoxide (in complexes **11–14**) is confirmed by the presence of a signal due to methyl protons at δ = 3.18–3.13 ppm.

^{13}C NMR spectral study

The coordination mode of the ligands in the complexes can be further elucidated by the measurement of ^{13}C NMR spectra (Table 5 and Fig. 12). Ligands **I**, **II**, **III** and **IV** exhibit 20, 18, 19 and 19 ^{13}C NMR signals against a total of 24, 22, 23 and 23 carbon atoms, respectively. Metal complexes exhibit normally the same or a higher number of signals compared to the ligands' spectra. Significant downfield shifts, $\Delta\delta$ = [δ(complex) − δ(ligand)], were observed for the carbon atoms present in the vicinity of the coordinating atoms O, N and O [*i.e.* pyrazolone oxygen (C1), azomethine nitrogen (C4) and enolic oxygen (C18)], confirming the coordination of these functionalities to the vanadium center. Signals due to methyl and other aromatic carbons (phenyl and pyrazol rings) appear in the expected δ values in the ligands' as well as in the complexes' spectra with slight variations. In complexes **11–14** a new signal appears at 68.3–72.4 ppm, which corresponds to the coordinated methoxy carbon atom.

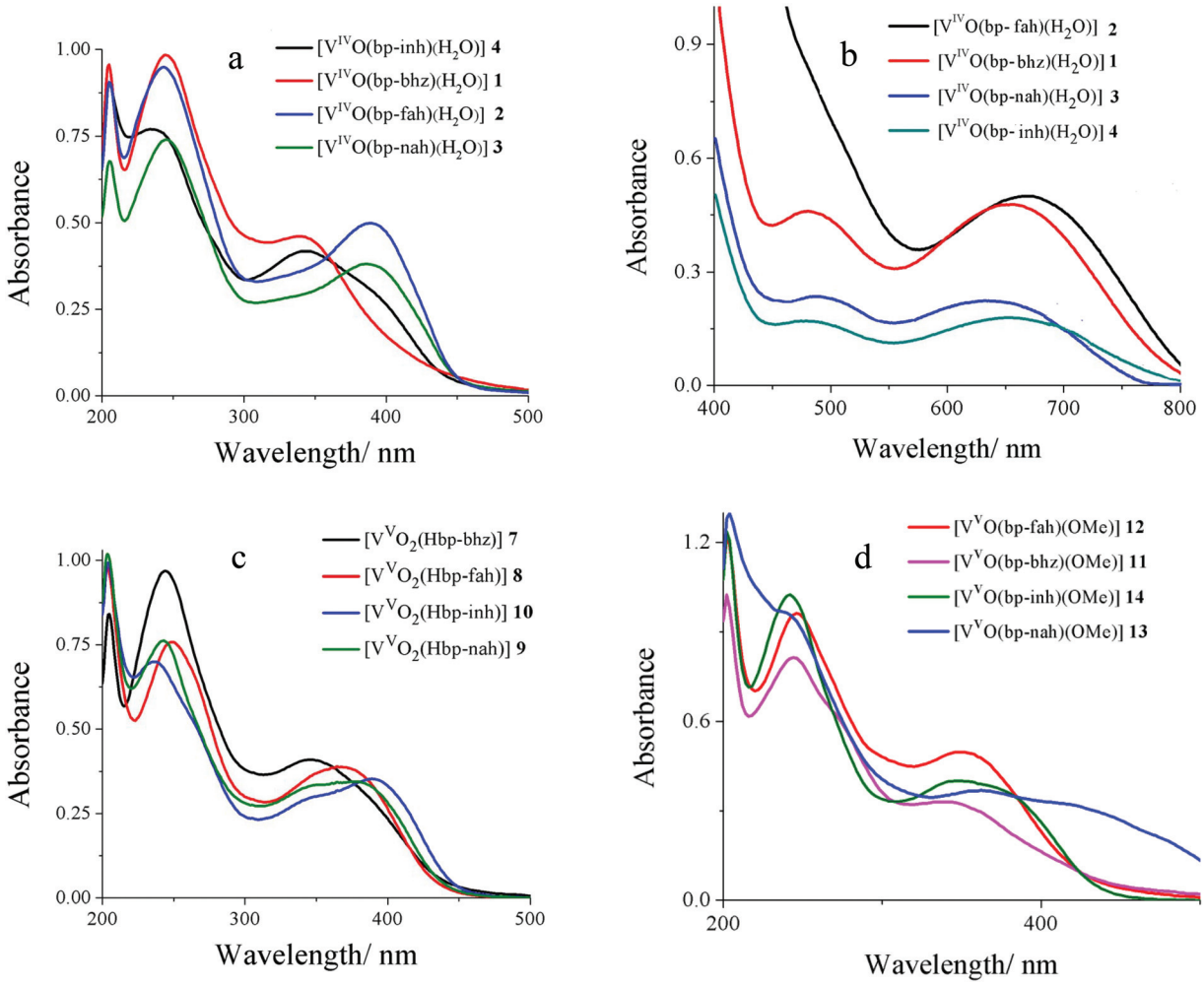

Fig. 10 (a) UV-vis spectra of the oxidovanadium(IV) complexes in methanol. Concentration 2.0 ± 0.2 × 10^{-4} M. (b) Vis spectra showing the d-bands of the oxidovanadium(IV) complexes in DMSO: **1** (conc. 4.4 × 10^{-3} M), **2** (conc. 3.9 × 10^{-3} M), **3** (conc. 2.5 × 10^{-3} M) and **4** (conc. 2.2 × 10^{-3} M). (c) UV-vis spectra of the dioxidovanadium(V) complexes in methanol: **7** (conc. 1.6 × 10^{-4} M), **8** (conc. 1.7 × 10^{-4} M), **9** (conc. 1.8 × 10^{-4} M) and **10** (conc. 1.9 × 10^{-4} M). (d) UV-vis spectra of the oxidomethoxidovanadium(V) complexes in methanol: **11** (conc. 1.3 × 10^{-4} M), **12** (conc. 1.9 × 10^{-4} M), **13** (conc. 2.1 × 10^{-4} M) and **14** (conc. 1.8 × 10^{-4} M).

^{51}V NMR spectral study

The complexes were further characterized by ^{51}V NMR spectroscopy in methanol (whenever soluble) and DMSO and Table 6 collects the spectra data. The line widths in MeOH are much lower than those in DMSO, as usual. Most complexes show one resonance in MeOH between −485.7 and −497.3 ppm; however, complexes **7** and **10** show three and two resonances, respectively. Typically, methoxy containing species resonate in the downfield region (below −500 ppm) since methanol and/or methoxy coordination increases the metal shielding, shifting the resonance to less negative values.[44] Table 6 includes also the chemical shift values measured for solutions of $V^{IV}O$-complexes **1–4** that were left under air for 1 day and which therefore correspond to oxidized species (+5). In DMSO all complexes show one broad resonance between −505.7 and −511.9 ppm and a few of them show a minor peak at *ca.* −480 ppm, which we assign to a decomposition product. The resonances are in the same chemical shift region as the previously reported acetyl pyrazolone complexes.[45]

EPR characterization

Complexes **1–4** were characterized by EPR spectroscopy; however the oxidation of complexes **1** and **2** precluded the determination of their spin Hamiltonian parameters, since very weak spectra were obtained for these two complexes in all tested solvents. For complexes **3** and **4** their spectra were measured in DMSO at 77 K, and they exhibit axial-type hyperfine patterns consistent with monomeric $V^{IV}O$-bound species with d^1_{xy} ground-state configuration – see Fig. S8.† They were simulated[36] and the following parameters were obtained for both complexes: $g_\perp$ = 1.984, $g_\parallel$ = 1.955, $A_\perp$ = 58.8 × 10^{-4} cm^{-1},

Table 4 ^{1}H NMR spectral data of ligands and vanadium(v) complexes recorded in DMSO-d_6

Compounds	–OH/–NH	Pyrazolone (CH)	CH_3	Ar–H
H_2ap-bhz **I**	11.00 (s, 1H)	1.45 (s, 1H)	1.42 (s, 3H)	8.00–7.98 (t, 2H), 7.97–7.94 (m, 2H), 7.70–7.68 (m, 1H), 7.63–7.53 (m, 2H), 7.52–7.38 (m, 8H)
$K(H_2O)_2[V^VO_2$(bp-bhz)] **5**			1.38 (s, 3H)	7.95–7.91 (d, 2H), 7.87–7.84 (m, 2H), 7.67–7.65 (m, 1H), 7.60–7.51 (m, 2H), 7.48–7.35 (m, 8H)
$[V^VO_2$(Hbp-bhz)] **7**			1.40 (s, 3H)	7.94–7.89 (d, 2H), 7.85–7.78 (m, 2H), 7.67–7.63 (m, 1H), 7.56–7.50 (m, 2H), 7.45–7.40 (m, 8H)
$[V^VO$(bp-bhz)(OMe)] **11**			1.43 (s, 3H)	8.00–7.95 (d, 2H), 7.91–7.86 (m, 2H), 7.78–7.75 (m, 1H), 7.58–7.52 (m, 2H), 7.49–7.45 (m, 8H)
H_2ap-fah **II**	10.96 (s, 1H)	1.48 (s, 1H)	1.38 (s, 3H)	8.01–7.97 (m, 2H), 7.82 (s, 1H), 7.69–7.40 (m, 8H), 7.09–7.08 (d, 1H), 6.59–6.58 (d, 1H)
$K(H_2O)_2[V^VO_2$(bp-fah)] **6**			1.34 (s, 3H)	7.84–7.82 (d, 2H), 7.62 (s, 1H), 7.52–7.41 (m, 5H), 7.23–7.19 (t, 1H), 6.71 (s, 1H), 6.48 (s, 1H)
$[V^VO_2$(Hbp-fah)] **8**			1.38 (s,3H)	7.84–7.82 (d, 2H), 7.62 (s, 1H), 7.52–7.41 (m, 5H), 7.23–7.19 (t, 1H), 6.71 (s, 1H), 6.48 (s, 1H)
$[V^VO$(bp-fah)(OMe)] **12**			1.40 (s, 3H)	7.84–7.82 (d, 2H), 7.62 (d, 2H), 7.37–7.31 (m, 6H), 7.23–7.19 (m, 3H)
H_2ap-nah **III**	11.20 (s, 1H)	1.46 (s, 1H)	1.42 (s, 3H)	8.69–8.61 (m, 2H), 8.01–7.87 (m, 3H), 7.70–7.67 (t, 1H), 7.62–7.40 (m, 8H)
$[V^VO_2$(Hbp-nah)] **9**			1.41 (s, 3H)	8.65–8.56 (m, 3H), 7.97–7.86 (m, 4H), 7.65–7.61 (t, 2H), 7.62–7.47 (m, 4H), 7.24 (s, 1H)
$[V^VO$(bp-nah)(OMe)] **13**			1.44 (s, 3H)	8.65–8.56 (m, 2H), 7.97–7.86 (m, 5H), 7.65–7.61 (t, 2H), 7.62–7.47 (m, 3H), 7.34 (d, 2H)
H_2ap-inh **IV**	11.46 (s, 1H)	1.47 (s, 1H)	1.41 (s, 3H)	8.78–8.66 (d, 2H), 7.99–7.91 (q, 2H), 7.86–7.67 (m, 2H), 7.62–7.40 (m, 8H)
$[V^VO_2$(Hbp-inh)] **10**			1.42 (s, 3H)	8.56 (s, 1H), 7.84–7.82 (d, 2H), 7.64–7.62 (d, 1H), 7.56–7.48 (m, 5H), 7.46–7.39 (m, 4H), 7.24–7.22 (t, 1H)
$[V^VO$(bp-inh)(OMe)] **14**			1.46 (s, 3H)	8.34–8.29 (q, 2H), 7.86–7.82 (m, 2H), 7.60–7.40 (m, 6H), 7.40–7.35 (m, 3H), 7.20–7.16 (t, 1H)

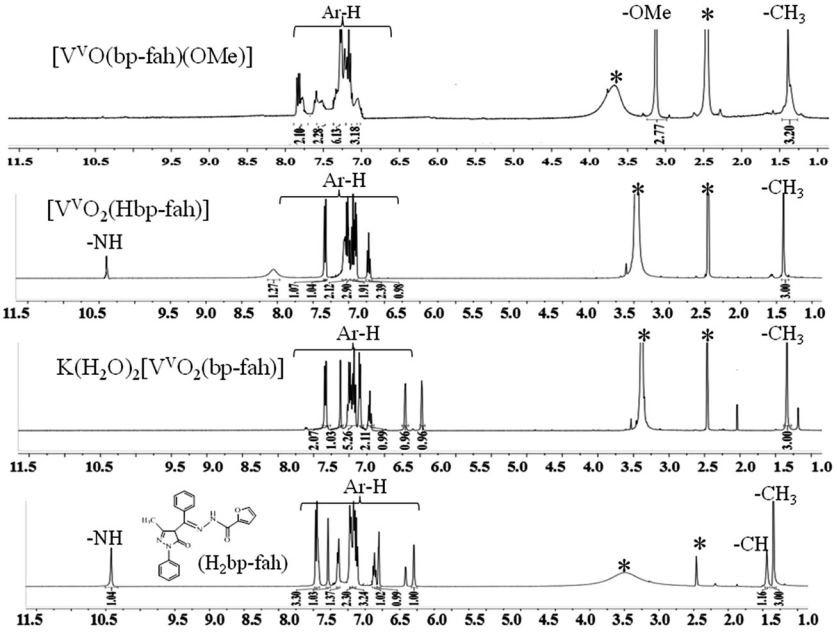

Fig. 11 ^{1}H NMR spectra of H_2bp-fah **II**, $K(H_2O)_2[V^VO_2$(bp-fah)] **6**, $[V^VO_2$(Hbp-fah)] **8** and $[V^VO$(bp-fah)(OMe)] **12** recorded in DMSO-d_6. The star (*) in the figure indicates the signal due to water in DMSO/DMSO itself.

$A_{\|} = 166.0 \times 10^{-4}$ cm^{-1}. These are quite similar to the ones obtained for the $V^{IV}O$ complexes containing ligands derived from the condensation of acetyl pyrazolone with nicotinoylhydrazide (nah) and isonicotinoylhydrazide (inh), previously reported by us.[45] Their coordination is the same and the spin Hamiltonian parameters are in agreement with a coordination mode including the enolic oxygen (of pyrazolone), the azomethine nitrogen, the enolic oxygen (hydrazide) and one water molecule.

Reactivity with H_2O_2

The reactivity pattern of the oxidovanadium(IV) complexes $[V^{IV}O(L)H_2O]$ **1–4** with aqueous 30% H_2O_2 in DMSO can be monitored by electronic absorption spectroscopy. The

Table 5 ^{13}C NMR spectral data of ligands and complexes recorded in DMSO-d_6

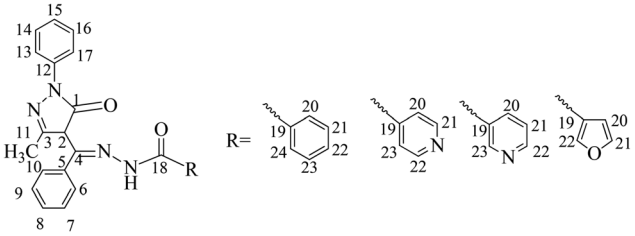

Compounds	C1	C4	C18	C2	C3	C11	Other aromatic carbon
H_2bp-bhz **I**	162.4	161.5	160.2	100	148.0	15.2	141.2, 139.1, 133.9, 131.6, 129.6, 129.1, 128.2, 109.1
$K(H_2O)_2[V^VO$(bp-bhz)] **5**	167.8	166.8	165.5	99.8	148.1	15.9	142.4, 139.1, 132.5, 130.3, 129.6, 128.5, 127.1, 108.8
($\Delta\delta$)	(5.4)	(5.3)	(5.3)				
$[V^VO_2$(Hbp-bhz)] **7**	166.9	166.4	165.9	100.5	147.9	15.6	142.4, 139.1, 133.5, 132.1, 129.1, 127.5, 127.1, 109.1
($\Delta\delta$)	(4.5)	(4.9)	(5.7)				
$[V^VO$(bp-bhz)(OMe)] **11**	166.4	167.3	164.8	100.3	148.4	16.1	143.1, 139.2, 132.6, 132.4, 130.1, 127.9, 126.1, 110.3
($\Delta\delta$)	(4.0)	(5.8)	(4.6)				
H_2bp-fah **II**	158.2	161.1	165.2	112.8	148.3	15.2	147.6, 146.8, 139.1, 137.8, 128.6, 128.2, 121.2
$K(H_2O)_2[V^VO$(bp-fah)] **6**	164.8	165.2	168.3	112.1	148.1	15.1	147.2, 145.2, 139.1, 136.2, 129.3, 128.2, 120.8
($\Delta\delta$)	(6.6)	(4.1)	(3.1)				
$[V^VO_2$(Hbp-fah)] **8**	166.4	165.2	168.6	111.8	147.9	15.7	147.1, 146.2, 138.8, 136.2, 128.8, 128.2, 121.8
($\Delta\delta$)	(8.2)	(4.1)	(3.5)				
$[V^VO$(bp-fah)(OMe)] **12**	166.2	166.4	168.4	112.0	148.3	16.2	148.4, 146.3, 139.5, 137.2, 129.8, 127.7, 122.5
($\Delta\delta$)	(8.0)	(4.3)	(3.2)				
H_2bp-nah **III**	162.1	159.3	157.6	101.2	148.9	15.8	147.4, 144.9, 140.1, 129.1, 124.8, 120.3, 112.4,
$[V^VO_2$(Hbp-nah)] **9**	166.3	163.8	161.9	101.6	148.4	17.1	147.1, 144.2, 139.6, 129.8, 125.2, 120.3, 112.1
($\Delta\delta$)	(4.2)	(4.5)	(4.3)				
$[V^VO$(bp-nah)(OMe)] **13**	167.3	165.1	163.6	101.9	147.9	16.9	148.3, 144.5, 140.1, 131.3, 125.8, 120.5, 115.3
($\Delta\delta$)	(5.2)	(5.8)	(6.0)				
H_2bp-inh **IV**	165.0	161.1	159.0	100.0	148.9	15.9	148.3, 138.2, 136.9, 130.1, 127.4, 124.8, 120.4
$[V^VO_2$(Hbp-inh)] **10**	168.6	164.9	163.8	101.1	149.1	15.6	148.1, 138.9, 136.3, 129, 1.128.0, 125.2, 120.4
($\Delta\delta$)	(3.6)	(3.8)	(4.9)				
$[V^VO$(bp-inh)(OMe)] **14**	170.2	165.4	163.7	101.2	148.0	16.4	149.2, 138.3, 138.3, 129.3, 128.2, 125.9, 122.1
($\Delta\delta$)	(5.2)	(4.3)	(4.7)				

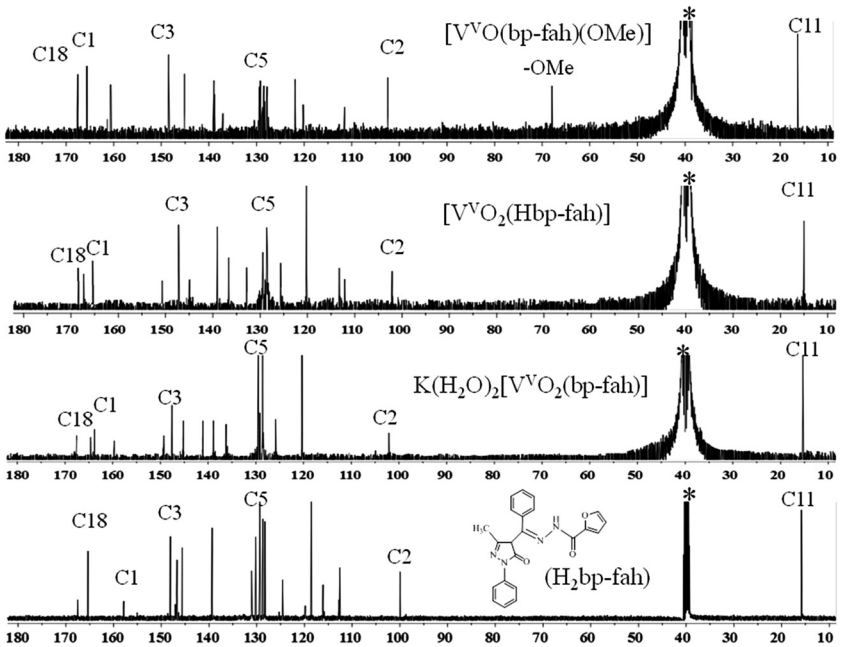

Fig. 12 ^{13}C NMR spectra of H_2bp-fah **II**, $K(H_2O)_2[V^VO_2$(bp-fah)] **6**, $[V^VO_2$(Hbp-fah)] **8** and $[V^VO$(bp-fah)(OMe)] **12** recorded in DMSO-d_6. The star (*) in the figure indicates the signal due to the carbon atoms of DMSO.

Table 6 ^{51}V NMR spectral data of complexes recorded in MeOH and DMSO

Compound	δ/ppm (ratio)	δ(ppm) (ratio)	δ(ppm) (ratio) After addition of H_2O_2	
	DMSO	MeOH	DMSO	MeOH
$[V^{IV}O(bp\text{-}bhz)(H_2O)]$ **1** [a]	−505.8	−486.5	−515.1	−534.1
$[V^{IV}O(bp\text{-}fah)(H_2O)]$ **2** [a]	−478.0(1) −509.7(8)	−493.6		−527.2
$[V^{IV}O(bp\text{-}nah)(H_2O)]$ **3** [a]	−506.7	—		—
$[V^{IV}O(bp\text{-}inh)(H_2O)]$ **4** [a]	−507.8	—		—
$K(H_2O)_2[V^{V}O_2(bp\text{-}bhz)]$ **5**	−506.7	−486.2	−550.0	−542.8
$K(H_2O)_2[V^{V}O_2(bp\text{-}fah)]$ **6**	−508.8	−492.6		−526.9
$[V^{V}O_2(Hbp\text{-}bhz)]$ **7**	−505.7	−485.7(5) −510.8(50) −547.1(1)		−571.7
$[V^{V}O_2(Hbp\text{-}fah)]$ **8**	−509.9	−493.4(6) −525.3(1)		−527.8
$[V^{V}O_2(Hbp\text{-}nah)]$ **9**	−506.7	−494.2	−517.0	−568.7
$[V^{V}O_2(Hbp\text{-}inh)]$ **10**	−507.4	−491.6(1) −513.4(10)	−518.9	−577.1
$[V^{V}O(bp\text{-}bhz)(OMe)]$ **11**	−479.9(1) −505.7(5)	−486.4		−533.0
$[V^{V}O(bp\text{-}fah)(OMe)]$ **12**	−479.2(1) −511.9(10)	−492.4		−526.3
$[V^{V}O(bp\text{-}nah)(OMe)]$ **13**	−509.1	−497.3		—
$[V^{V}O(bp\text{-}inh)(OMe)]$ **14**	−507.2	−491.9	−517.0	−576.4

[a] After oxidation under air.

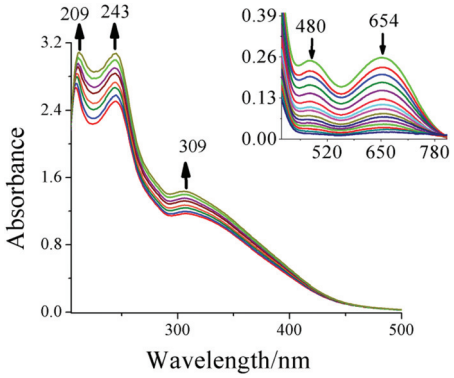

Fig. 13 UV-vis spectral changes observed during the titration of $[V^{IV}O(bp\text{-}bhz)H_2O]$ **1** with H_2O_2. The spectra were recorded upon stepwise additions of one-drop portions of H_2O_2 (2.2×10^{-2} M) to 2.5×10^{-4} M solution of **1** in DMSO. The inset shows spectral changes observed for the d-bands of complex **1** in DMSO upon addition of H_2O_2. The spectra were recorded upon stepwise addition of two-drop portions of H_2O_2 (2.1×10^{-2} M) to 25 mL of a 3.4×10^{-3} M solution of **1** in DMSO.

changes observed upon progressive addition of one-drop portions of a 2.2×10^{-2} M 30% H_2O_2 solution to 2.5×10^{-4} M $[V^{IV}O(bp\text{-}bhz)H_2O]$ **1** in DMSO are presented in Fig. 13. The intensity of the bands appearing at 209, 243 and 309 nm slowly increases. At higher concentration (*ca.* 10^{-3} M), complex **1**, which exhibits two bands at 480 and 654 nm (inset of Fig. 13), shows the flattening and subsequent disappearance of these bands upon addition of H_2O_2. All these changes indicate the oxidation of oxidovanadium(IV) complex to a higher oxidation state. Very similar spectral changes were observed upon treatment of $[V^{IV}O(bp\text{-}fah)H_2O]$ **2** with aqueous H_2O_2, Fig. S9.†

For complexes $K(H_2O)_2[V^{V}O_2(bp\text{-}bhz)]$ **5**, the intensity of the ligand centered bands increases while the LMCT band suffers changes. Simultaneously, an isosbestic point also appears which indicate the formation of a new species, probably involving coordination of the peroxide, Fig. 14.

The oxidation was also monitored by ^{51}V NMR spectroscopy and Table 6 contains the collected data. Upon the addition of an aqueous 30% solution of H_2O_2 to the methanolic solutions of the complexes (*ca.* 3 mM) the resonance at *ca.* −485 ppm progressively disappears and a new resonance appears between *ca.* −525 and −580 ppm (see Fig. 15a) for complex **9**. We tentatively assign this species to a peroxidovanadate complex of the type $[V^{V}O_2(O_2)(L)]^-$.[46] The complexes containing the furoyl substituent (**2**, **6**, **8** and **12**) are the ones that resonate more downfield, while the ones containing pyridine resonate upfield, due to electronic effects. When excess H_2O_2 is added a peak is observed at *ca.* −650 ppm, which we assign to an inorganic diperoxidovanadate, $[V^{V}O(O_2)_2]^-$.[47]

In DMSO the chemical shifts of the oxidovanadium(V) or dioxidovanadium(V) complex and the diperoxidooxidovandium(V) complex are quite similar and due to the larger linewidths of the complexes' resonances; for complexes **6–9** the peaks are indistinguishable and only an increase in the peak linewidth is observed upon addition of H_2O_2 (see the example of complex **9** in Fig. S11(a)†). However, for complex **10** it is clear that a new peak appears slightly upfield, upon addition of H_2O_2 to the complex solution in DMSO – see Fig. 15(b). The same happens for a few other complexes. Fig. S12† presents the spectra obtained after addition of H_2O_2 into both solvents.

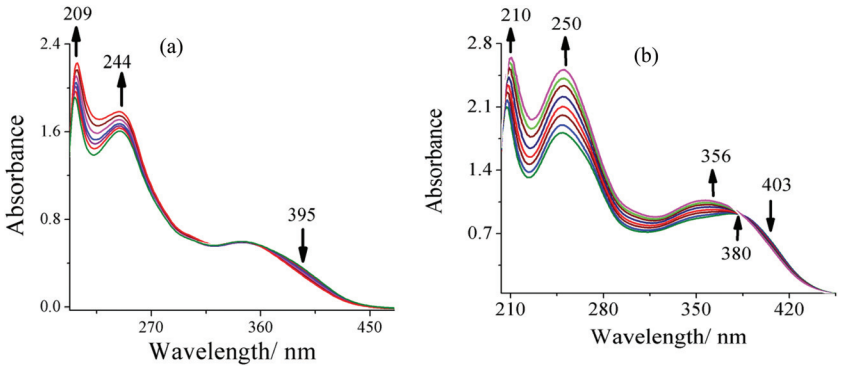

Fig. 14 (a): UV-vis spectral changes observed during the titration of a methanolic solution of $K(H_2O)_2[V^VO_2(bp\text{-}bhz)]$ **5** with H_2O_2. The spectra were recorded upon stepwise addition of one-drop portions of 30% H_2O_2 (2.1×10^{-2} M) to 25 mL of 3.2×10^{-4} M solution in MeOH. (b) UV-vis spectral changes observed during the titration of $K(H_2O)_2[V^VO_2(bp\text{-}fah)]$ **6** with H_2O_2. The spectra were recorded upon stepwise addition of one-drop portions of H_2O_2 (2.8×10^{-2} M) to 25 mL of 2.3×10^{-4} M solution in MeOH.

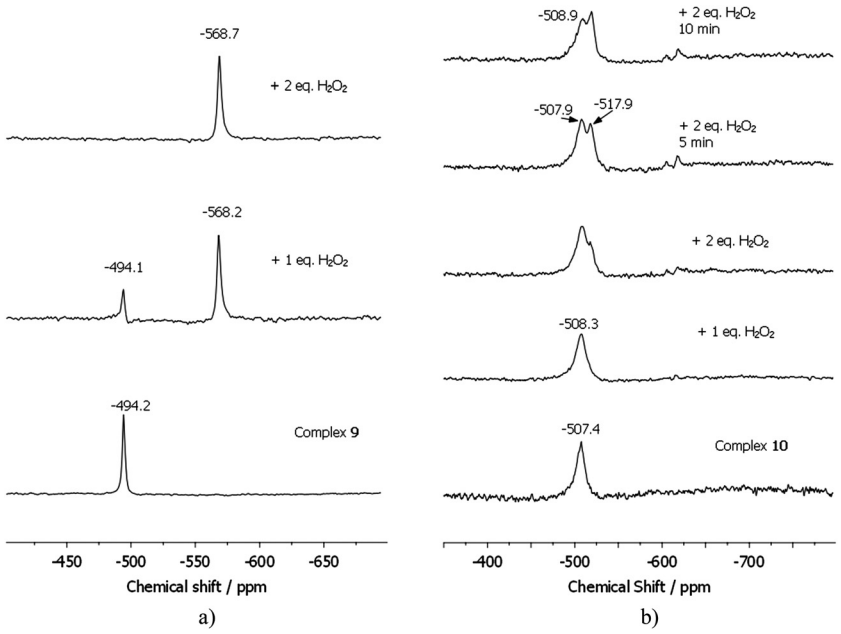

Fig. 15 ^{51}V NMR spectra recorded for *ca.* 3 mM solutions of the complexes before and after addition of different amounts of H_2O_2. (a) Complex **9** in MeOH and (b) complex **10** in DMSO.

Catalytic activity

Recently studied $[MoO_2]^{2+}$ and $[MoO(O_2)]^{2+}$ complexes catalyzed the multi-component Hantzsch reaction using the reactants benzaldehyde, methylacetoacetate and ammonium acetate, resulting in the formation of two products: (a) dimethyl 2,6-dimethyl-4-phenylpyridine-3,5-dicarboxylate and (b) dimethyl 2,6-dimethyl-4-phenyl-1,4-dihydropyridine-3,5-dicarboxylate under solvent free conditions, Scheme 3.[48] 88% conversion of combined reaction products with *ca.* 90% selectivity for dihydropyridine (a) at 40 °C and relatively lower conversion with *ca.* 99% selectivity of dihydropyridine (a) at 60 °C under optimized reaction conditions were obtained. In the present investigation this multi-component reaction catalyzed by oxidovanadium(v) complexes **11–14** under solvent free conditions also gave two products with very similar selectivities.

In order to understand the reactivity and selectivity of the resulting products, the effects of the amounts of catalyst, H_2O_2, solvent, and temperature were studied taking $[V^VO(bp\text{-}bhz)(OMe)]$ **11** as a representative catalyst precursor.

In a systematic study, three different amounts (*i.e.* 0.0010 g, 0.0020 g and 0.0030 g) of catalyst precursor (complex **11**) were added to a mixture of benzaldehyde (0.53 g, 0.0050 mol), ethylacetoacetate (1.3 g, 0.010 mol), ammonium acetate (0.46 g, 0.005 mol) and aqueous 30% H_2O_2 (0.55 g, 0.005 mol) and the reaction mixture (under solvent free conditions) was stirred at 30 °C for 1 hour. Increasing the catalyst amount from 0.0010 g to 0.0020 g leads to a conversion increase from 67% to 88%;

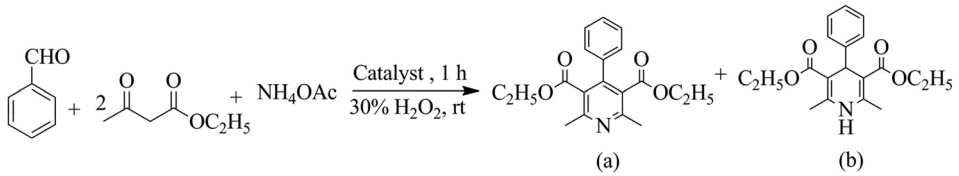

Scheme 3 Multi-component aromatization of substituted-1,4-dihydropyridines at room temperature.

Table 7 Conversion of multiple components (0.0050 mol of benzaldehyde, 0.010 mol of ethylacetoacetate and 0.0050 mol of ammonium acetate) into products (a) and (b) using [$V^{V}O$(bp-bhz)(OMe)] as catalyst precursor in 1 h of reaction time under different reaction conditions

Entry no	Catalyst amount g (μmol)	Oxidant amount g (mol)	Temp. (°C)	Solvent	% Conv.	% Selectivity		TOF
						a	*b*	
1	0.0010 (2.0)	0.55 (0.0050)	30	—	67	97	3	837
2	0.0020 (4.0)	0.55 (0.0050)	30	—	88	96	4	1100
3	0.0030 (6.0)	0.55 (0.0050)	30	—	91	97	3	1137
4	0.0020 (4.0)	1.1 (0.010)	30	—	93	93	7	1162
5	0.0020 (4.0)	1.7 (0.015)	30	—	93	99	1	1162
6	0.0020 (4.0)	0.55 (0.0050)	40	—	89	92	8	1112
7	0.0020 (4.0)	0.55 (0.0050)	50	—	91	90	10	1137
8	0.0020 (4.0)	0.55 (0.0050)	60	—	92	89	11	1150
9	0.0020 (4.0)	0.55 (0.0050)	70	—	94	87	13	1175
10	0.0020 (4.0)	0.55 (0.0050)	30	CH_3CN	85	88	12	1062
11	0.0020 (4.0)	0.55 (0.0050)	30	MeOH	80	90	10	1000
12	0.0020 (4.0)	0.55 (0.0050)	30	EtOH	81	87	13	1012
13	0.0020 (4.0)	0.55 (0.0050)	30	$CHCl_3$	75	80	20	937
14	0.0020 (4.0)	0.55 (0.0050)	30	CH_2Cl_2	77	75	24	962
15	0.0020 (4.0)	0.55 (0.0050)	30	Hexane	73	72	27	912
16	0.0020 (4.0)	Blank	30	—	49	82	18	
17	Blank	0.55 (0.0050)	30	—	30	85	15	

however, further increasing the amount to 0.0030 g does not improve much either the conversion or the product selectivity (entries 1–3 of Table 7 and Fig. S13(a)).†

The effect of the amount of oxidant (30% aqueous H_2O_2) is illustrated in Fig. S13(b).† For 0.0020 g of catalyst under the above reaction conditions, a substrate to oxidant ratio of 1 : 1 gave 88% conversion with 96% selectivity for pyridine derivative (a). Increasing the ratio to either 1 : 2 or 1 : 3 did not improve much the conversion (93%), while the selectivity for the pyridine derivative (a) was improved (entries 2, 4 and 5 of Table 7) slightly, reaching 99% at a substrate to oxidant ratio of 1 : 3. Therefore, a substrate to H_2O_2 ratio of 1 : 1 was considered suitable to further optimize the other parameters.

Fig. S13(c)† illustrates the temperature effect as a function of time under the above optimized reaction conditions. From the figure we can conclude that 30 °C is the best temperature for achieving maximum yield and selectivity. At this temperature, *ca*. 88% conversion was achieved in 1 h of contact time. At higher temperatures, *viz*. 40, 50, 60 and 70 °C, the conversions were *ca*. 90%, as well as the selectivity (entries 6–9 of Table 7). Therefore, on increasing the temperature the overall conversion does not change much while the selectivity slightly decreases.

Thus, entry 2 of Table 7 shows the best-suited reaction conditions to obtain a good yield of the combined products with 96% of pyridine derivative (a) in 1 h of reaction time. However, as high as 99% selectivity of the pyridine derivative could be achieved under the reaction conditions mentioned in entry 5 of Table 7.

Solvents such as EtOH, MeOH, CH_3CN, CH_2Cl_2 and $CHCl_3$ were also tested to see their overall effect (entries 10–15 of Table 7). Among these, CH_3CN, MeOH, and EtOH gave 80, 82 and 83% conversion, respectively, with 88–90% selectivity of pyridine derivative (a) (see Scheme 3), whereas reaction in CH_2Cl_2, $CHCl_3$ and hexane gave lower yields of 75, 77 and 73%, respectively, and selectivities between 72 and 80%. The generation of the catalytically active species, oxidoperoxidovanadium(v), by the interaction of the vanadium complex with H_2O_2 is probably affected by the polarity of the solvent. We can hypothesize that the active species is stabilized in polar aprotic solvents like CH_3CN due to coordination of the solvent to the metal core center,[49] therefore giving higher conversion. The polar protic solvents MeOH and EtOH can coordinate strongly to the metal center, giving less active species, which are possibly responsible for the lower reaction yields.[50] On the other hand, the nonpolar solvent hexane and chlorinated solvents like CH_2Cl_2 and $CHCl_3$, which do not have coordinating power, give rise to lower activity.

In the absence of the catalyst, the reaction was very slow and an overall 30% conversion was achieved in 1 h of reac-

Table 8 Conversion, TOF and product selectivity by catalyst **11–14** under optimized reaction conditions

S. no.	Catalyst (μmol)	% Conv.	TOF/h^{-1}	% Selectivity of product a
1	$[V^{V}O(bp\text{-}bhz)(OMe)]$ **11** (4.0)	88	1100	96
2	$[V^{V}O(bp\text{-}fah)(OMe)]$ **12** (4.1)	91	1137	94
3	$[V^{V}O(bp\text{-}nah)(OMe)]$ **13** (4.0)	89	1112	98
4	$[V^{V}O(bp\text{-}inh)(OMe)]$ **14** (4.0)	90	1125	93

Table 9 Effect of various substituents on the benzaldehyde multi-component substrate on the conversion and selectivity of different products under optimized reaction conditions

Entry no.	Substrates	% Conv.	TOF/h^{-1}	% Selectivity of product (a)
1	4-Methylbenzaldehyde	95	1187	95
2	Salicylaldehyde	93	1162	94
3	4-*t*-Methylbenzaldehyde	96	1200	96
4	4-Methoxybenzaldehyde	96	1200	93
5	2-Nitrobenzaldehyde	75	937	97
6	2-Chlorobenzaldehyde	70	875	99

tion at room temperature under the above optimized reaction conditions. Clearly, the catalyst is an essential component for this reaction. The oxidation was also tested in the absence of H_2O_2 but in the presence of catalyst, which gave 49% conversion. All these clearly indicate that the catalyst, as well as the oxidant, is required to enhance substantially the aromatization process.

We have also studied the catalytic potential of the other three oxidomethoxidovanadium(v) complexes (**12**, **13** and **14**) in the multi-component Hantzsch reaction and Table 8 summarizes the results. Thus, all catalysts show similar catalytic behaviour with conversion values within 88–91% and selectivity values within 93–98%, under the optimised reaction conditions.

To evaluate the substrate scope the substituent effect on benzaldehyde was studied, considering the reaction at 30 °C using complex **11** as a catalyst precursor. The results are summarized in Table 9. The introduction of electron donating substituents *i.e.* methoxy, methyl, *t*-butyl and OH on benzaldehyde results in slightly higher conversion, with 93–96% selectivity of pyridine derivative, while electron withdrawing groups, like

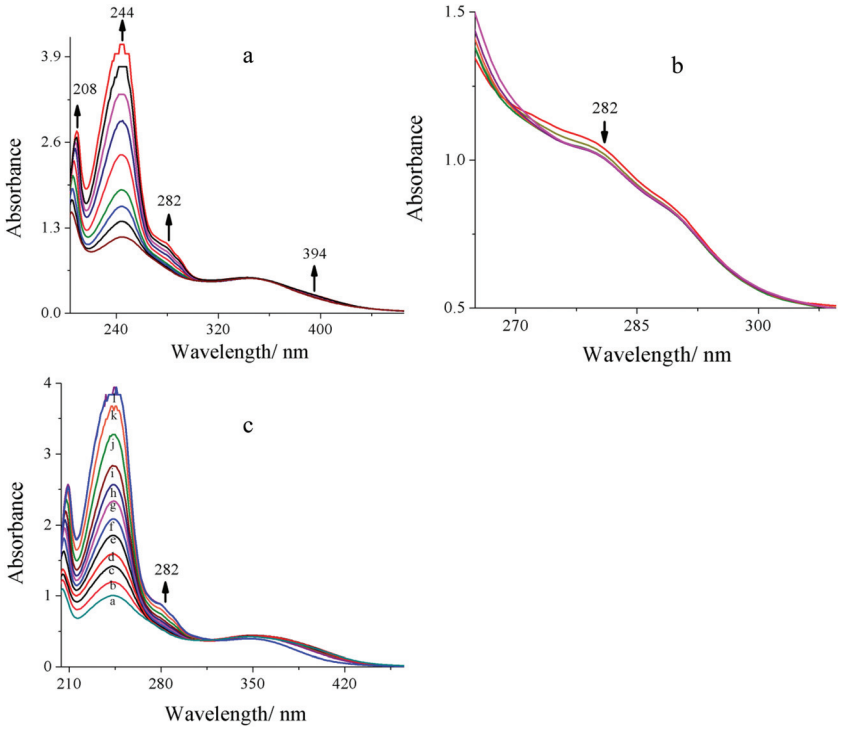

Fig. 16 (a) Spectral changes observed after the successive addition of one-drop portions of 1.4×10^{-2} M benzaldehyde dissolved in 10 mL of MeOH to 10 mL of a (2.3×10^{-4} M) solution of $[V^{V}O(bp\text{-}bhz)(OMe)]$; (b) spectral changes observed after the successive addition of one-drop portions of methanolic solution of H_2O_2 (1.9×10^{-2} M) to the above solution; (c) spectral changes (a–f) observed after the successive addition of one-drop portions of 1.9×10^{-2} M of H_2O_2 (final conc.) dissolved in 10 mL of MeOH to 10 mL of a (2.4×10^{-4} M) solution of $[V^{V}O(bp\text{-}bhz)(OMe)]$, and spectral changes (g–l) observed after successive addition of one-drop portions of (benzaldehyde + ethyacetoacetate) (2.6×10^{-2} M) to the above solution.

chloro and nitro, result in much lower conversion (70–75%), with 97–99% selectivity of the pyridine derivative.

Possible reaction route for Hantzsch reaction

To establish the possible route for the vanadium catalyzed Hantzsch reaction, the interaction between benzaldehyde and catalyst [$V^{V}O$(bp-bhz)(OMe)] **11** was studied. Thus, initially 20 mL of a solution of **11** (2.3×10^{-4} M) in MeOH were treated with one-drop portions of 1.4×10^{-2} M benzaldehyde solution in MeOH and the resulting spectroscopic changes are presented in Fig. 16(a). The intensity of all the UV bands increases. In addition, a new band at 282 nm appears, suggesting an interaction between benzaldehyde and complex **11**. The dropwise addition of a methanolic solution of ethylacetoacetate (1.5×10^{-2} M) to the above solution of **11** results only in a slight intensity increase of the existing 282 nm band. This possibly indicates the weak interaction of the acidic hydrogen atom (*i.e.* active methylene hydrogen) of ethylacetoacetate with the lone pair of electrons present on nitrogen atoms of the ligand system of complex **11**. Upon dropwise addition of a (1.9×10^{-2} M) methanolic solution of H_2O_2 to the above solution, the intensity of the band at 282 nm slightly decreases, indicating that the interaction between catalyst and benzaldehyde decreases and the catalyst is regenerated (see the steps of intermediate **I** in Scheme 4).

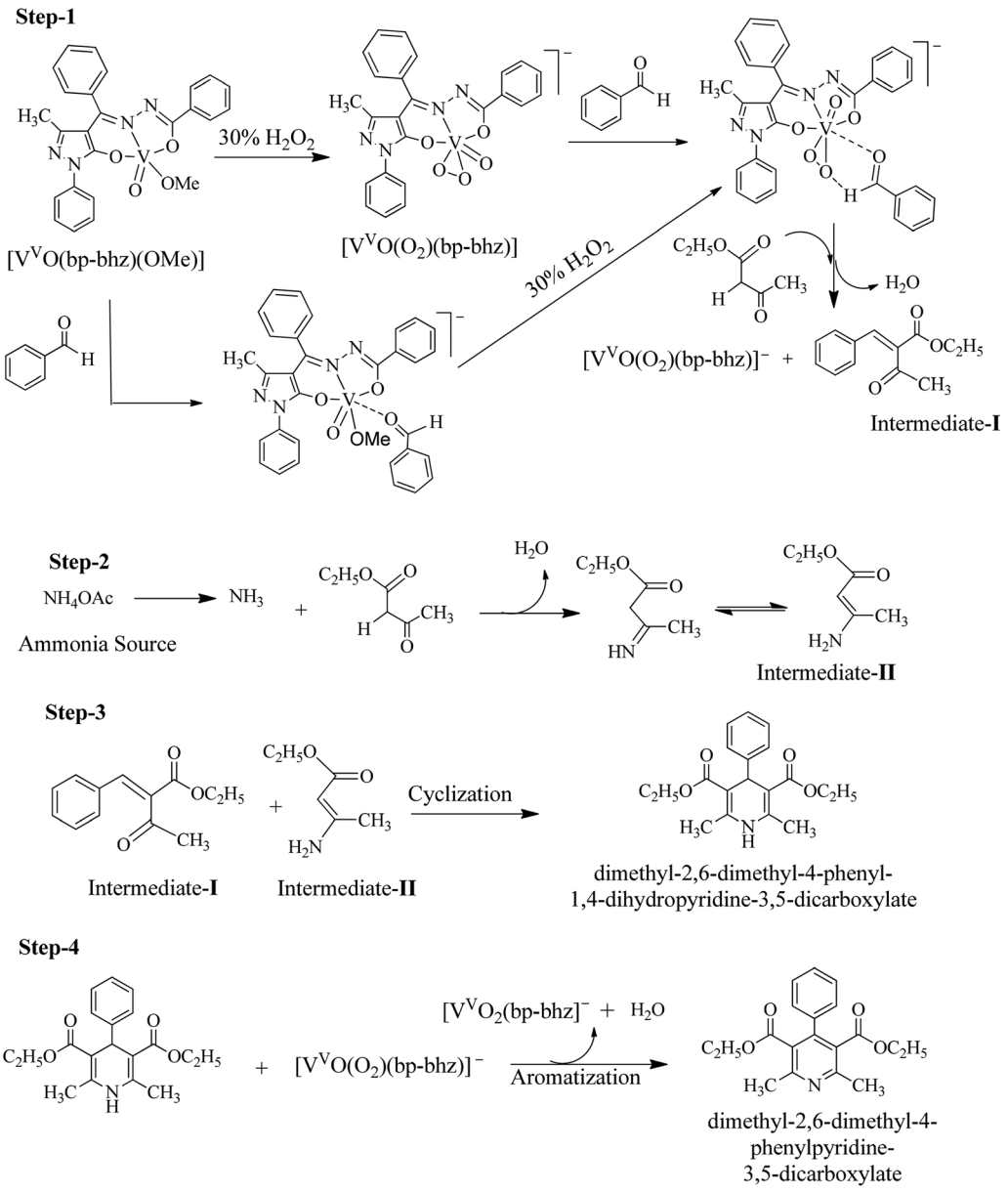

Scheme 4 Plausible mechanism for the formation of diethyl 2,6-dimethyl-4-phenyl-1,4-dihydropyridine-3,5-dicarboxylate and the corresponding diethyl 2,6-dimethyl-4-phenylpyridine-3,5-dicarboxylate.

Also, the dropwise addition of 1.9×10^{-2} M H_2O_2 in MeOH to a 2.4×10^{-4} M methanolic solution of **11** shows the formation of oxidoperoxidovanadium(v) species [spectra a–f in Fig. 16c]. A new band at 282 nm appears after the dropwise addition of a mixture of (2.6×10^{-2} M benzaldyde + ethylacetoacetate) to the above solution, suggesting the interaction of benzaldehyde with oxidoperoxidovanadium(v) species. All these observations probably suggest the interaction of complex **11**, as well as its oxidoperoxidovanadium(v) intermediate, with benzaldehyde, followed by its reaction with activated ethylacetoacetate to give the Knoevenagel condensation product as an intermediate **I**.[48] Based on these observations the following mechanism (steps 1–4) is suggested for the three-component one-pot Hantzsch reaction: the non-catalytic step 2, involving the interaction of the second molecule of ethylacetoacetate with ammonium acetate[51] to give intermediate **II**, and the interaction of intermediates **I** and **II** in step 3 to give dihydropyridine[48] are obvious. Finally, the catalytic conversion of dihydropyridine into the corresponding pyridine (*i.e.* step 4) occurs.[21,52]

The catalytic Hantzsch reaction using benzaldehyde, methylacetoacetate/ethylacetoacetate and ammonium acetate by the catalysts reported here compares very well with other catalysts reported in the literature, *e.g.* the V_2O_5/H_2O_2 [23a] system, which gives 96% conversion in CH_3CN at room temperature with 96% selectivity towards pyridine derivative, and the vanadium salt, $VOCl_3$,[23b] which gives 97% conversion in CH_2Cl_2 with 97% selectivity towards pyridine derivative.

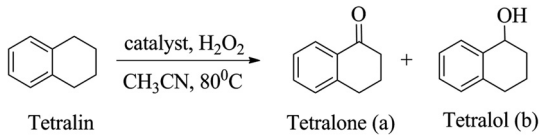

Scheme 5 Oxidation products of tetralin using [V^{V}O(bp-bhz)(OMe)] **11** as catalyst.

Oxidation of tetralin

The catalytic potential of the vanadium complexes for the oxidation of tetralin in the presence of 30% H_2O_2 as oxidant has also been investigated (see Scheme 5). The formation of α-tetralone[49] (main product) and α-tetralol (minor product) has been identified in the test reaction.

In order to optimize the reaction conditions for the maximum conversion of tetralin into products, several parameters such as the amounts of catalyst, H_2O_2, solvent and temperature have been studied in detail using [V^{V}O(bp-bhz)(OMe)] **11** as a representative catalyst. Thus, for 1.3 g (0.010 mol) of tetralin, three different amounts of catalyst (0.0010, 0.0020, and 0.0030 g) (entries 1–3) and 30% aqueous H_2O_2 (0.010, 0.020, and 0.030 mol) (entries 4 and 5) were taken in three different volumes of the solvent MeCN (*i.e.* 5, 7, and 10 mL) (entries 6 and 7), and the reactions were carried out at three different temperatures (*i.e.* 60, 70, and 80 °C) (entries 8 and 9) for 8 h. Fig. S14† presents details of the reactions' progress under various conditions and Table 10 summarizes the results obtained.

It is clear that entries 5–7 of Table 10 are the best suited reaction conditions to obtain *ca.* 65% oxidation of tetralin to the major product, α-tetralone, with 96–97% selectivity in *ca.* 8 h of reaction time. Therefore, entry 5, with the lowest solvent amount, was selected as the best one.

The solvent effect on the oxidation of tetralin was studied using MeOH, EtOH, CH_2Cl_2, $CHCl_3$ and hexane (entries 10–14 of Table 10). All these solvents gave much lower conversions than MeCN, under similar reaction conditions, with $CHCl_3$, CH_2Cl_2 and hexane performing even worse than MeOH and EtOH.

We have also tested the catalytic potential of the other three oxidomethoxidovanadium(v) complexes (**12–14**) for the oxidation of tetralin under the optimized reaction conditions mentioned above and Table 11 summarizes the results, as well as the turnover frequency. All catalysts show similar behaviour with conversion values within 57–64%. A blank reaction under these conditions (*i.e.* without catalyst) gave only 11% conver-

Table 10 Oxidation of tetralin (1.3 g, 0.010 mol) obtained under different reaction conditions using [V^{V}O(bp-bhz)(OMe)] **11** as catalyst under different reaction conditions

							Selectivity		
Entry no.	Tetralin [g (mol)]	H_2O_2 [g (mol)]	Catalyst [g (μmol)]	MeCN (mL)	Temp.	% Conv.	*a*	*b*	TOF
1	1.3 (0.010)	2.3 (0.020)	0.0010 (2.0)	5	80	38	90	10	119
2	1.3 (0.010)	2.3 (0.020)	0.0020 (4.0)	5	80	51	92	8	159
3	1.3 (0.010)	2.3 (0.020)	0.0030 (6.0)	5	80	54	93	7	168
4	1.3 (0.010)	1.1 (0.010)	0.0020 (4.0)	5	80	33	88	12	103
5	1.3 (0.010)	3.4 (0.030)	0.0020 (4.0)	5	80	64	97	3	200
6	1.3 (0.010)	3.4 (0.030)	0.0020 (4.0)	7	80	65	96	4	203
7	1.3 (0.010)	3.4 (0.030)	0.0020 (4.0)	10	80	66	96	4	206
8	1.3 (0.010)	3.4 (0.030)	0.0020 (4.0)	5	60	32	90	10	100
9	1.3 (0.010)	3.4 (0.030)	0.0020 (4.0)	5	70	48	89	11	150
10	1.3 (0.010)	3.4 (0.030)	0.0020 (4.0)	MeOH	80	53	92	8	200
11	1.3 (0.010)	3.4 (0.030)	0.0020 (4.0)	EtOH	80	51	94	6	200
12	1.3 (0.010)	3.4 (0.030)	0.0020 (4.0)	$CHCl_3$	80	45	87	13	200
13	1.3 (0.010)	3.4 (0.030)	0.0020 (4.0)	CH_2Cl_2	80	42	89	10	200
14	1.3 (0.010)	3.4 (0.030)	0.0020 (4.0)	Hexane	80	40	88	12	200
15	1.3 (0.010)	3.4 (0.030)	—	5	80	11	90	10	

Table 11 Conversion, TOF and product selectivity under the optimised reaction conditions

S. no.	Catalyst (μmol)	% Conv.	TOF/h^{-1}	% Selectivity of α-tetralone
1	$[V^{V}O(bp\text{-}bhz)(OMe)]$ **11**(4.0)	64	200	97
2	$[V^{V}O(bp\text{-}fah)(OMe)]$ **12** (4.1)	62	193	95
3	$[V^{V}O(bp\text{-}nah)(OMe)]$ **13** (4.0)	60	187	92
4	$[V^{V}O(bp\text{-}inh)(OMe)]$ **14** (4.0)	57	178	94

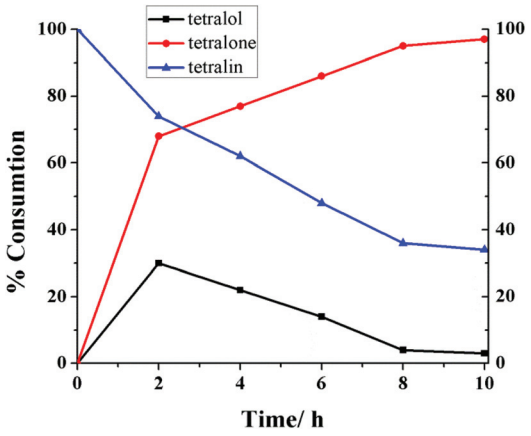

Fig. 17 Profile showing % consumption of tetralin along with % selectivity of the formation of products tetralone and tetralol using catalyst $[V^{V}O(bp\text{-}bhz)(OMe)]$ under the optimized reaction conditions (entry no. 5 of Table 10).

sion. Thus, all complexes show catalytic activity for the oxidation of tetralin.

The variation of the catalyzed consumption of tetralin and formation of α-tetralone and α-tetralol with time was recorded. As presented in Fig. 17 the selectivity for the formation of α-tetralone starts with the consumption of tetralin, increases with time and reaches 97% after 8 h of reaction time. The selectivity of α-tetralol is higher in the first 2 h, then declines and after 8 h decreases to 3%. We can conclude that there are two processes for the formation of tetralone, one of them involving the transformation of α-tetralol into α-tetralone.

As far as we know, no vanadium complexes have been reported in the literature to catalyze the oxidation of tetralin. $Cu[(bpy)_2Cl]Cl$ [53] in the presence 30% H_2O_2 gives 55% conversion, whereas catalysts $[MnCl_2(P(2\text{-}py)_3)(OH_2)]\cdot 2H_2O$, $[Co(P(2\text{-}py)_3)_2]Cl_2\cdot 2MeOH$ and $[NiCl_2(P(2\text{-}py)_3)(OH_2)]\cdot H_2O$ [$P(2\text{-}py)_3$ = tris(2-pyridyl)phosphine][50] give 51, 42 and 44% conversion, respectively. Catalysts $[Cu(CTZ)_4]Cl_2$ [54] and $K_8HP_2V_3W_{15}O_6\cdot 9H_2O$ [55] give 52 and 50% conversion in the presence of oxygen, respectively. Thus, the catalytic oxidation of tetralin by catalysts reported herein compares well with the literature.

Conclusions

The use of different starting precursors and reaction conditions yields different vanadium complexes of general compositions: $[V^{IV}OL(H_2O)]$, $\{[K(H_2O)_2][V^{V}O_2L]\}_2$, $[V^{V}O_2(HL)]$ and $[V^{V}OL(OMe)]$ (H_2L = dianionic ONO ligands derived from the condensation of 4-benzoyl-3-methyl-1-phenyl-2-pyrazoline-5-one (Hbp) with benzoylhydrazide (H_2bp-bhz **I**), furoylhydrazide (H_2bp-fah **II**), nicotinoylhydrazide (H_2bp-nah **III**) and isonicotinoylhydrazide (H_2bp-inh **IV**)). All complexes were characterized by elemental analysis and spectroscopic techniques. The molecular structure of complexes $K(H_2O)_2[V^{V}O_2(bp\text{-}bhz)]$ **5**, $K(H_2O)_2[V^{V}O_2(bp\text{-}fah)]$ **6**, $[V^{V}O_2(Hbp\text{-}bhz)]$ **7**, $[V^{V}O_2(Hbp\text{-}fah)]$ **8** to $[V^{V}O_2(Hbp\text{-}nah)]$ **9**, $[V^{V}O_2(Hbp\text{-}inh)]$ **10** and $[V^{V}O(bp\text{-}fah)(OMe)]$ **12** was elucidated by single crystal X-ray diffraction analyses. Complexes **5** and **6** are not isostructural around K ions but present cation–π interactions between the phenyl ring of the ligand and the K^+ ion, which control the assembly in dimeric aggregates. In complexes **7** and **8** the protonation takes place at the hydrazide nitrogen, whereas in complexes **9** and **10** such a protonation occurs at the pyridine nitrogen. The $[V^{V}OL(OMe)]$ type complexes **11–14** catalyze the Hantzsch reaction, a one-pot three-component (ethylacetoacetate, benzaldehyde and ammonium acetate) dynamic covalent assembly, in the presence of hydrogen peroxide (30% H_2O_2) as oxidant, in solution and under solvent free conditions. These complexes also show excellent catalytic activity towards the oxidation of tetratlin to tetralone.

Acknowledgements

MRM thanks the Science and Engineering Research Board (SERB), Government of India, New Delhi for financial support of this work (EMR/2014/000529). BS is thankful to IIT Roorkee for awarding a MHRD fellowship. I. Correia acknowledges Fundação para a Ciência e Tecnologia for an Investigator FCT contract, UID/QUI/00100/2013, and the IST-UTL Centers of the Portuguese NMR.

References

1 G. Grün and A. Fleckenstein, *Arzneim. Forsch. (Drug Res.).*, 1972, **22**, 334–344.
2 T. Tsuruo, H. Iida, M. Nojiri, S. Tsukagoshi and Y. Sakurai, *Cancer Res.*, 1983, **43**, 2905–2910.
3 R. W. Chapman, G. Danko and M. I. Siegels, *Pharmacology*, 1984, **29**, 282–291.
4 W. J. Malaise and P. C. F. Mathias, *Diabetologia*, 1985, **28**, 153–156.
5 A. Krauze, S. Germane, O. Eberlins, I. Sturms, V. Klusa and G. Duburs, *Eur. J. Med. Chem.*, 1999, **34**, 301–310.

6 R. Peri, S. Padmanabhan, S. Singh, A. Rutledge and D. J. Triggle, *J. Med. Chem.*, 2000, **43**, 2906–2914.
7 A. Hantzsch, *Justus Liebigs Ann. Chem.*, 1882, **215**, 1–82.
8 G. Sabitha, G. S. K. K. Reddy, C. S. Reddy and J. S. Yadav, *Tetrahedron Lett.*, 2003, **44**, 4129–4131.
9 B. Khadikar and S. Borkat, *Synth. Commun.*, 1998, **28**, 207–212, and references cited therein.
10 R. H. Bocker and F. P. Guengerich, *J. Med. Chem.*, 1986, **29**, 1596–1603.
11 H. Bischhoff, R. Angerbauer, J. Bender, E. Bischoff, A. Faggiotto, D. Petzinna, J. Pfitzner, M. C. Porter, D. Schmidt and G. Thomas, *Atherosclerosis*, 1997, **135**, 119–130.
12 J. J. V. Eynde, A. Mayence and A. Maquestiau, *Tetrahedron*, 1992, **48**, 463–468.
13 G. Sabitha, G. S. K. K. Reddy, C. S. Reddy, N. Fatima and J. S. Yadav, *Synthesis*, 2003, 1267–1271.
14 J. R. Pfister, *Synthesis*, 1990, 689–690.
15 H. R. Memarian, M. Abdoli-Senejani and S. Tangestaninejad, *J. Iran. Chem. Soc.*, 2006, **3**, 285–292.
16 M. A. Zolfigol, M. Kiany-Borazjani, M. M. Sadeghi, I. Mohammadpoor- Baltork and H. R. Memarian, *Synth. Commun.*, 2000, **30**, 551–558.
17 N. Nakamichi, Y. Kawashita and M. Hayashi, *Synthesis*, 2004, 1015–1020.
18 M. Filipan-Litvić, M. Litvić and V. Vinković, *Tetrahedron*, 2008, **64**, 5649–5656.
19 M. Nasr-Esfahani, M. Moghadam and G. Valipour, *Synth. Commun.*, 2009, **39**, 3867–3879.
20 T. Shamim, M. Gupta and S. Paul, *J. Mol. Catal. A: Chem.*, 2009, **302**, 15–19.
21 M. Litvić, M. Regović, K. Šmic, M. Lovrić and M. Filipan-Litvić, *Bioorg. Med. Chem. Lett.*, 2012, **22**, 3676–3681.
22 M. Filipan-Litvić, M. Litvić, I. Cepanec and V. Vinkovi, *ARKIVOC*, 2008, 96–103.
23 (*a*) M. Filipan-Litvić, M. Litvić and V. Vinković, *Tetrahedron*, 2008, **64**, 10912–10918; (*b*) J. Su, C. Zhang, D. Lin, Y. Duan, X. Fu and R. Mu, *Synth. Commun.*, 2010, **40**, 595–600.
24 (*a*) M. R. Maurya, A. K. Chandrakar and S. Chand, *J. Mol. Catal. A: Chem.*, 2007, **263**, 227–237; (*b*) S. Barroso, P. Adão, F. Madeira, M. T. Duarte, J. Costa Pessoa and A. M. Martins, *Inorg. Chem.*, 2010, **49**, 7452–7463.
25 M. R. Maurya, C. Haldar, A. A. Khan, A. Azam, A. Salahuddin, A. Kumar and J. Costa Pessoa, *Eur. J. Inorg. Chem.*, 2012, 2560–2577.
26 B. N. Wigington, M. L. Drummond, T. R. Cundari, D. L. Thorn, S. K. Hanson and S. L. Scott, *Chem. – Eur. J.*, 2012, **18**, 14981–14988.
27 M. R. Maurya and N. Kumar, *J. Mol. Catal. A: Chem.*, 2014, **383–384**, 172–181.
28 M. R. Maurya, A. Kumar and J. Costa Pessoa, *Coord. Chem. Rev.*, 2011, **255**, 2315–2344.
29 A. Covarrubias-Zuniga, F. Cantu and L. A. Maldonado, *J. Org. Chem.*, 2008, **63**, 2918–2921.
30 H. G. Frank and J. W. Stadelhofer, *Industrial Aromatic Chemistry*, Springer-Verlag, Berlin, Heidelberg, 1988.
31 G. A. Olah, *Friedel-Crafts and Related Reactions*, Wiley-Interscience, New York, 1963.
32 (*a*) M. Grzywa, C. Geßner, B. Bredenkötter, D. Denysenko, J. Leusen, P. Kögerler, E. Klemm and D. Volkmer, *Dalton Trans.*, 2014, **43**, 16846–16856; (*b*) R. A. Shaikh, G. Chandrasekar, K. Biswas, J.-S. Choi, W.-J. Son, S.-Y. Jeong and W.-S. Ahn, *Catal. Today*, 2008, **132**, 52–57.
33 M. Zhu, X. Wei, B. Li and Y. Yuan, *Tetrahedron Lett.*, 2007, **48**, 9108–9111.
34 R. A. Rowe and M. M. Jones, *Inorg. Synth.*, 1957, **5**, 113–116.
35 M. R. Maurya, N. Saini and F. Avecilla, *RSC Adv.*, 2016, **6**, 12993–13009.
36 A. Rockenbauer and L. Korecz, *Appl. Magn. Reson.*, 1996, **10**, 29–43.
37 G. M. Sheldrick, *SADABS, version 2.10*, University of Göttingen, Germany, 2004.
38 G. M. Sheldrick, SHELX, *Acta Crystallogr., Sect. A: Fundam. Crystallogr.*, 2008, **64**, 112–122.
39 L. J. Farrugia, *J. Appl. Crystallogr.*, 1999, **32**, 837–838.
40 M. M. Hänninen, A. Peuronen, P. Damlin, V. Tyystajärvi, H. Kivelä and A. Lehtonen, *Dalton Trans.*, 2014, **43**, 14022–14028.
41 J. J. Morris, B. C. Noll, G. W. Honeyman, C. T. ÓHara, A. R. Kennedy, R. E. Mulvey and K. W. Henderson, *Chem. – Eur. J.*, 2007, **13**, 4418–4432.
42 P. Adão, M. R. Maurya, U. Kumar, F. Avecilla, R. T. Henriques, M. L. Kusnetsov, J. Costa Pessoa and I. Correia, *Pure Appl. Chem.*, 2009, **81**, 1279–1296.
43 I. Correia, J. Costa Pessoa, M. T. Duarte, R. T. Henriques, M. F. M. Piedade, L. F. Veiros, T. Jakusch, T. Kiss, Á. Dörnyei, M. Margarida, C. A. Castro, C. F. G. C. Geraldes and F. Avecilla, *Chem. – Eur. J.*, 2004, **10**, 2301–2317.
44 D. Rehder, C. Weidemann, A. Duch and W. Priebsch, *Inorg. Chem.*, 1988, **27**, 584–587.
45 M. R. Maurya, B. Sarkar, F. Avecilla and I. Correia, *Eur. J. Inorg. Chem.*, 2016, 4028–4044.
46 V. Conte, F. Di Furia and S. More, *Inorg. Chim. Acta*, 1998, **272**, 62–67.
47 C. Slebodnick and V. L. Pecoraro, *Inorg. Chim. Acta*, 1998, **283**, 37–43.
48 (*a*) O. D'Alessandro, Á. G. Sathicq, J. E. Sambeth, H. J. Thomas and G. P. Romanelli, *Catal. Commun.*, 2015, **60**, 65–69; (*b*) Y. Liu, J. Liu, X. Wang, T. Cheng and R. Li, *Tetrahedron*, 2013, **69**, 5242–5247; (*c*) H. Khabazzadeh, I. Sheikhshoaie and S. Saeid-Nia, *Transition Met. Chem.*, 2010, **35**, 125–127.
49 A. N. Kharat, B. T. Jahromi and A. Bakhoda, *Transition Met. Chem.*, 2012, **37**, 63–69.
50 C. Wang, Y. Zhang, B. Yuan and J. Zhao, *J. Mol. Catal. A: Chem.*, 2010, **333**, 173–179.
51 (*a*) A. Saini, S. Kumar and J. S. Sandhu, *J. Sci. Ind. Res.*, 2008, **67**, 95–11; (*b*) L. Shen, S. Cao, J. Wu, J. Zhang, H. Li, N. Liu and X. Qian, *Green Chem.*, 2009, **11**, 1414–1420; (*c*) A. Debache, W. Ghalem, R. Boulcina, A. Belfaitah, S. Rhouati and B. Carboni, *Tetrahedron Lett.*, 2009, **50**, 5248–5250.

52 M. Sharbatdaran, L. J. Foruzin, F. Farzaneh and M. M. Larijani, *C. R. Chim.*, 2013, **16**, 176–182.
53 B. Louis, C. Detoni, N. M. F. Carvalho, C. D. Duarte and O. A. C. Antunes, *Appl. Catal., A*, 2009, **360**, 218–225.
54 M. Navarro, A. Escobar, V. R. Landaeta, G. Visbal, F. Lopez-Linares, M. L. Luis and A. Fuentes, *Appl. Catal., A*, 2009, **363**, 27–31.
55 R. Razi, M. Abedini, A. N. Kharat and M. M. Amini, *Catal. Commun.*, 2008, **9**, 245–249.